NUMERICAL PREDICTION OF ATMOSPHERIC BLOCKING

A CASE STUDY

L. Bengtsson

European Centre for Medium
Range Weather Forecasts,
England

Seminar 1979

1. INTRODUCTION

One of the fundamental questions in dynamical meteorology and one of the basic objectives of GARP, is to determine the predictability of the atmosphere. In the early planning stage and preparation for GARP a number of theoretical and numerical studies were undertaken, indicating that there existed an inherent unpredictability in the atmosphere which even with the most ideal observing system would limit useful weather forecasting to 2 - 3 weeks. Charney et al (1966), Lorenz (1968), (1969a) and (1969b), Robinson (1967) and Smagorinsky (1969). In particular it was found that an initial random error increased in time, with a doubling of the error in 3 to 5 days, the error growth being faster for small errors. It was also found that the theoretical error growth was scale dependent with a much higher predictability for the larger scales than for the smaller scales. According to Lorenz (1969b), who carried out a theoretical predictability study for a barotropic model, the predictability for a 20000 km wave is almost four times larger than a 5000 km wave.

In the numerical experiments summarised by Charney et al (1966) and by Smagorinsky (1969), a random perturbation was added to a prescribed initial state and the forecast from the perturbed initial state was compared with a reference prediction without the error. The predictability was investigated by studying how the 2 predictions deviated from each other during the course of the integration. The predictability was defined as the time when the two forecasts differed as much as two randomly chosen states.

Assuming the random frequency distribution it can be shown that the difference between two randomly chosen states has an RMS difference which is $\sqrt{2}$ times larger than the climatic variance, Thompson (1961). The original definition of predictability has therefore little practical meaning and we will as has been suggested by Döös (1970), in this

article use the term useful predictability which is the time when the prediction error reaches the climatic variance. In the evaluation of a series of 10-day prediction experiments at ECMWF, Hollingsworth et al (1979) used this definition of useful predictability and found that it agreed quite well with an independent subjective evaluation. A corresponding value for the correlation (anomaly correlation) was found to be around 0.6.

Prediction experiments using real data are less favourable than the numerical simulations. Experiments reported by Miyakoda (1972), Druyan et al (1975) and Hollingsworth et al (1979) give a value of the useful predictability of 4 - 5 days, the latest experiment having a slightly better value.

A closer examination of the prediction error from numerical forecasts in general shows several interesting features.

(i) The error growth in the beginning of the forecast is substantially higher in the real integrations.

(ii) The predictability for the ultra-long waves is, at least for some prediction models, less than for the medium scale waves.

(iii) All numerical models, known to the author, produce systematic errors with a characteristic geographical distribution common for most models.

(iv) There is a considerable variation in predictability from day to day and from episode to episode.

The rapid error growth at the beginning of the forecast is most likely caused by an inaccurate specification of the initial state, in particular phase errors can cause a very rapid growth of the initial error. Bengtsson (1978).

The high growth rate of the ultra-long waves seems to be a problem mainly for models with an insufficient resolution (either horizontal or vertical) or oversimplified physical parameterization. Lambert and Merilees (1978) have investigated the Canadian spectral operational model and found that in that particular model at that particular time the medium scale waves were better predicted than the ultra-long waves. There are also indications, Somerville (1979), that a lateral boundary condition at the equator and an unsatisfactory treatment of the data in the Tropical belt will reduce the predictability of the long waves. We will comment on this particular question later in this investigation. There are indications that the very poor results for the ultra-long waves disappear when more advanced models are being used. The ECMWF model for instance clearly predicts the ultra-long waves better than the medium scale waves.

The systematic errors are related to the errors in the long waves because they have a very large-scale geographical distribution and consequently large-scale systematic errors show up as errors in the long waves. These errors are most noticeable in the winter and a common feature is to predict too high geopotential values in the western part of the Atlantic and too low values in the eastern Atlantic. A similar error distribution can be found in the Pacific.

Perhaps the most puzzling prediction problem is the very large variation of predictability with time. Fig. 1 shows the result of seven integrations carried out at ECMWF, Hollingsworth et al (1979) with a high resolution global grid point model. The forecasts were all from February 1976 and based upon analyses from NMC Washington, using data from DST-6. In spite of the fact that for this period we had a homogeneous observational data set the useful predictability varied from less than 5 days to beyond 8 days. Integrations using a different parameterization

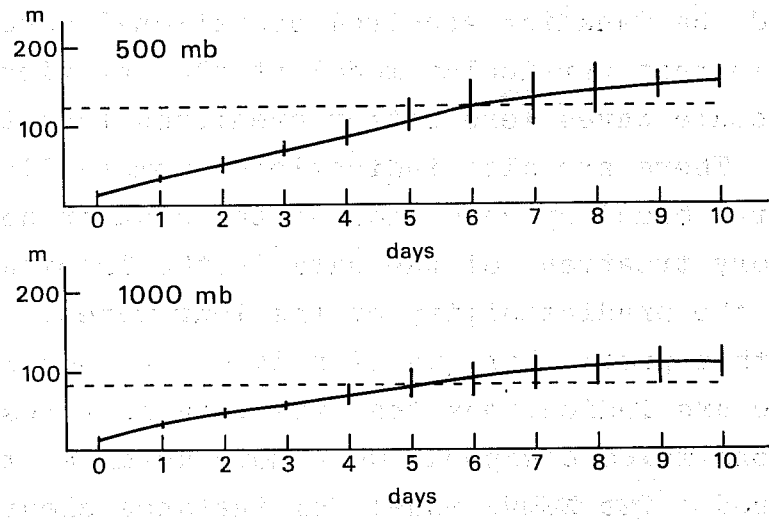

Fig. 1 The thin line shows the ensemble RMS-error for the surface and 500 mb as a function of time for 7 different forecasts from February 1976. The vertical line shows the variability in the RMS-error day by day. The horizontal dashed line is the climatic norm.

and high resolution spectral models gave a similar picture and it has been clearly demonstrated that on certain days all forecasts were poor while on other days in general all forecasts were good.

The most successful forecast among the 7 cases investigated at ECMWF was a prediction of a typical blocking pattern. Fig. 2 shows the forecast from 15/2/1976. As can be seen, the characteristic blocking pattern over northern Europe is predicted in a very accurate way. The result of this integration and other successful predictions of blocking is both very interesting and very encouraging. It is interesting because it suggests that a blocking pattern may be regarded as a sort of a quasi-stable equilibrium as has been suggested by Charney and DeVore (1979). Such an equilibrium can be generated by a non-linear interaction between some large scale components together with a necessary forcing from topography and by non-adiabatic processes. Charney and DeVore considered a simple barotropic low-order system with topography and Newtonian forcing. In the real atmosphere the effect of topography and non-adiabatic processes is much more complicated and the energy of the large scale systems is to a major extent obtained through energy transfer from the baroclinic waves. This process can be represented by Newtonian forcing only to a very limited degree. It is unlikely that we will have an equilibrium in the real atmosphere but instead a repetitive characteristic evolution of a certain weather pattern.

Successful forecasting of blocking is of utmost practical importance. The largest deviation from climatology occurs during blocking situations. With blocking occurring over northern Europe or the northeastern Atlantic in the winter, outbreaks of very cold Arctic air to the south of the block often generates intensive small-scale depressions with strong winds and heavy snow falls. Such weather events can create serious disruption in the society and are of

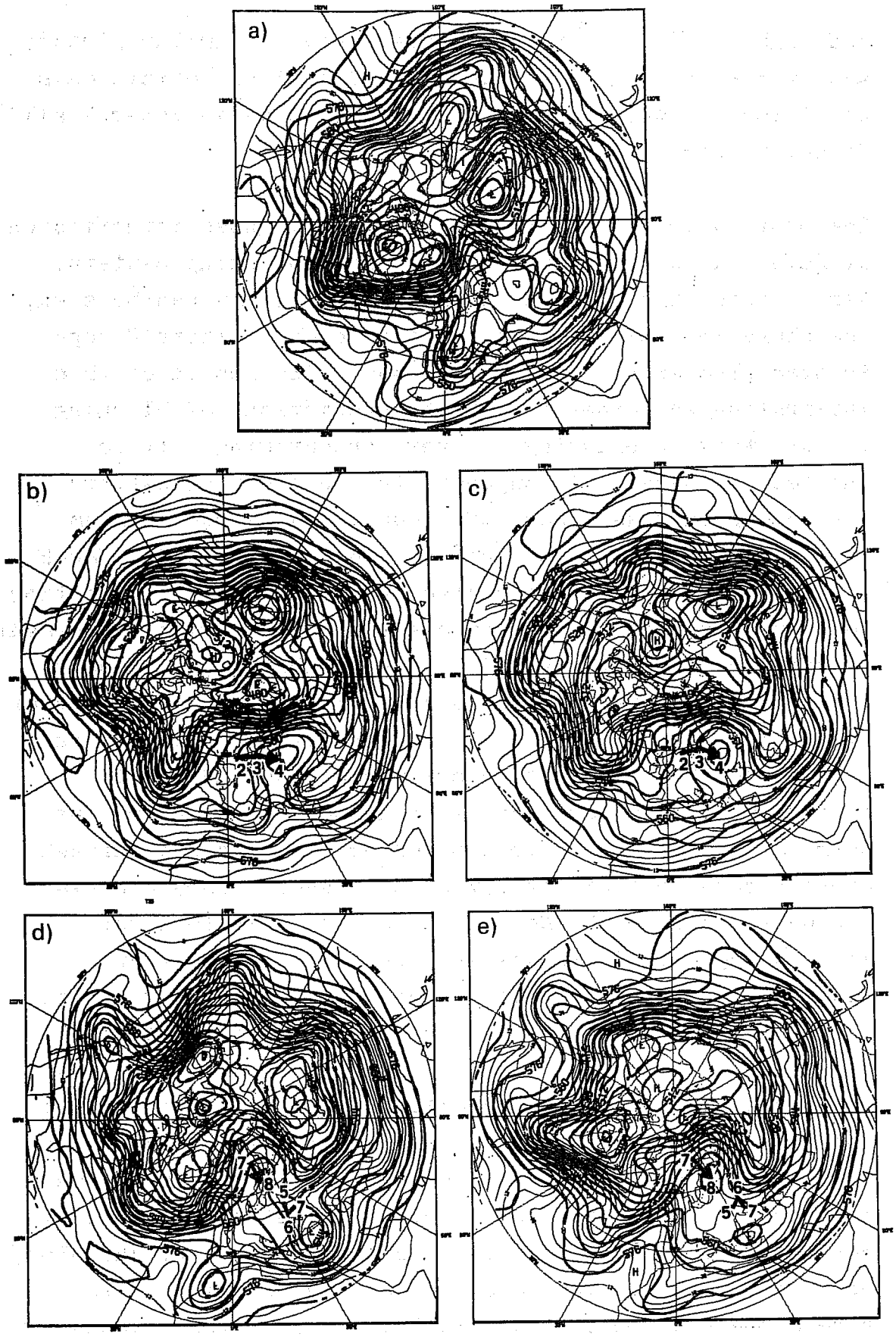

Fig. 2 500 mb geopotential (full lines) and the 500 mb temperatures (thin lines) for the forecast for 15/2/1976 00Z (a) the initial state, (b) 4 day prediction (c) verification 19/2 00Z, (d) 8 day prediction (e) verification 23/2 00Z. Thick lines on maps (b)-(e) show the predicted and the observed motion of the blocking high for each individual day. This forecast was the most successful of the 7 cases from DST-6 mentioned in the text.

greatest importance to be predicted as far in advance as possible.

The winter of 1979 was characterised by a very high frequency of blocking in the eastern Atlantic. Associated with the blocking, periods of very cold and unsettled weather with several disastrous snow storms occurred in northern and central Europe. The purpose of this study is to carry out an investigation of a particular forecast for 16/1/1979 00Z which turned out to be exceptionally accurate for as far as 8 days ahead, and which showed useful predictability for more than 12 days. By a successive simplification of the model we will further try to indicate what the essential conditions are for the prediction of the blocking pattern in this particular case. In the first part of this study we will describe in detail one high resolution integration. In the second part we will present results from simplified models and show how a successive simplification of the models as well as a reduction of the data being used gives rise to a deterioration of the forecast.

2. SYNOPTIC DESCRIPTION

The weather situation preceding 16/1/1979 is characterised by a well-defined zonal flow over the Atlantic and western Eurasian sector. The zonal flow is successively breaking down and on the 16/1/1979 two cut-off lows are created at 40 ^{o}N, one at 15 ^{o}W and another one at 25 ^{o}E. In particular the cut-off low over eastern Europe is very intense. The flow pattern during the following eight days develops into a typical blocking situation. See Fig. 3.

The ridge over western Europe moves during the first 2 days towards north-northwest under gradual intensification. The axis of the ridge then swings over from a north-south orientation to a west-east and moves slowly into a quasi-stationary position over central Scandinavia where it stays during day 3 - 5. A very intense cyclone develops west of

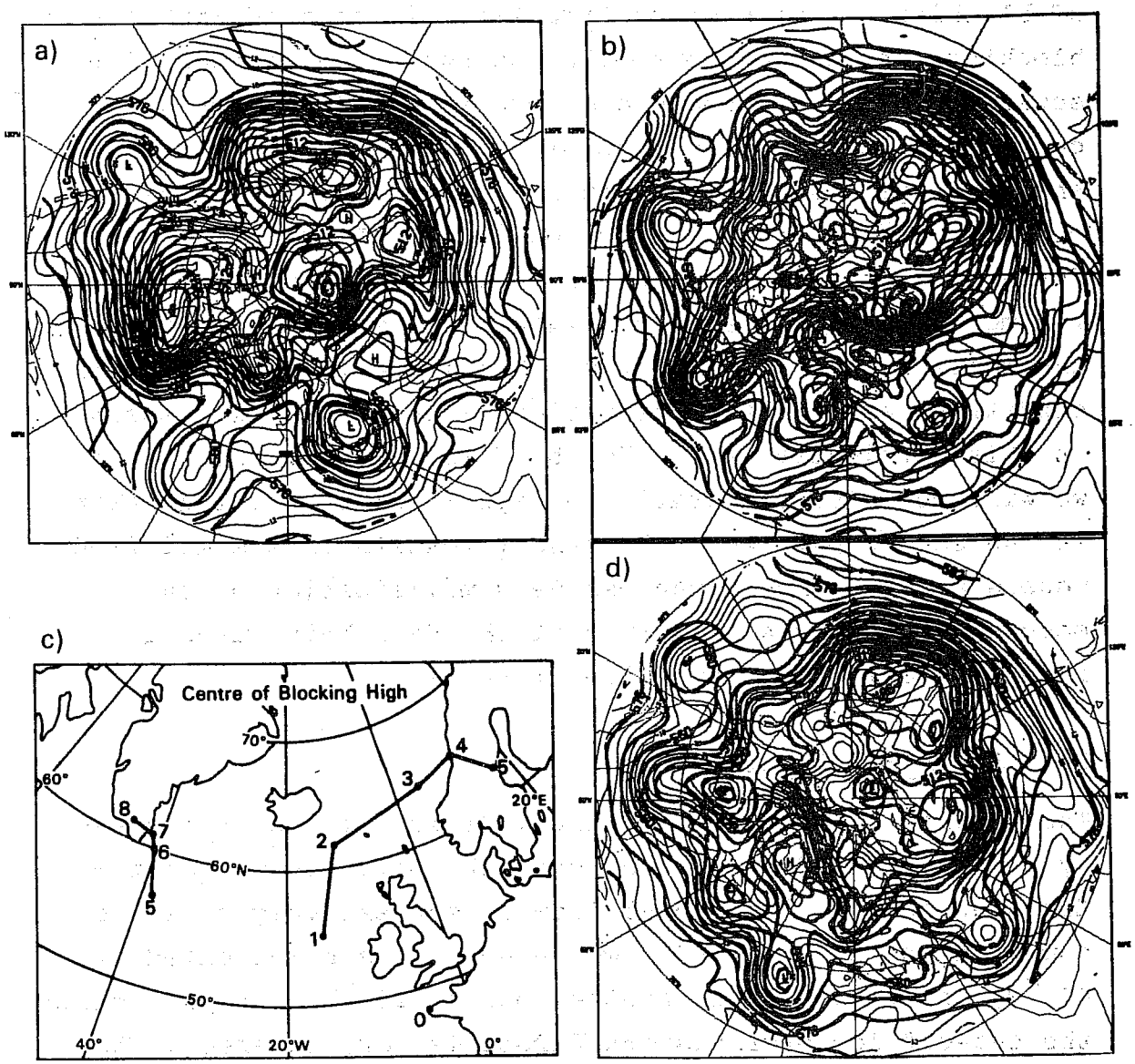

Fig. 3 500 mb geopotential (full lines) and temperatures (thin lines) for 16/1/1979 00Z (a), 20/1 00Z (b) and 24/1 00Z (d).
Figure 3c shows the motion of the blocking high day by day.

Spitzbergen on day 3 and moves eastward on the north side of this ridge. This cyclone plays an essential role in intensifying the northern branch of the jet to the north of the high pressure over Scandinavia. Over southern Europe the two cut-off lows have merged into large areas of cyclonic activity, and the westerly jet over Northern Africa is also successively intensified.

The 500 mb flow of day 4 shows a characteristic blocking pattern with a split of the jet around 40 W and a blocking pattern over central Scandinavia. The flow pattern from day 3 onwards fulfils the criteria for blocking according to Rex (1950a), (1950b), namely

- The basic westerly current is split into two branches
- Each branch current is transporting an appreciable mass
- The double jet is extending over at least 45^{o} lon
- A sharp transition from a zonal flow upstream to a meridional type downstream is observed at the current split.

At day 5 the high pressure weakens suddenly over Scandinavia and a new high is established around 40 ^{o}W. This high pressure constitutes a new blocking cell. This new cell is amplified and drifts slowly towards north-northwest during the next couple of days. There is a substantial cyclone activity to the west of this ridge and it is suggested that the northward transport of heat and momentum plays an active role in building up this new high pressure cell.

3. THE INITIAL DATA

The initial data for this case were obtained from a preliminary data assimilation experiment carried out at ECMWF using FGGE level III-b data from 15 - 19 January 1979. In this experiment all FGGE level III-b data were not available and the major addition to the operational data from the GTS were winds from the five geostationary satellites and data from the microwave sounder from TIROS N.

The data assimilation was carried out by an intermittent 4-dimensional assimilation scheme. The frequency of data insertion was 6 hours, and observations within 3 hours of the analysis time were assumed to be synoptic. The analysis was done by a 3-dimensional statistical multivariate scheme, Lorenc et al (1977). Every analysis was initialised by a non-linear normal mode technique described by Temperton and Williamson (1979). The prediction model used in the data assimilation was the gridpoint model of ECMWF, Burridge and Haseler (1977) and Tiedtke et al (1979). The horizontal resolution was 1.875^{o} lat/lon staggered grid and the vertical resolution consisted of 15 levels in the vertical. Table 1 shows the vertical levels. The data assimilation started 13/1/1979 00Z and climatology was used as the first guess for the very first analyses in the series. The data assimilation experiment continued for several days but the prediction experiment to be described below have all been done from 16/1/1979 00Z. Where not particularly mentioned, the initial data for the different integrations have been interpolated from the initial gridpoint data.

15-level model		5-level model	
k	σ_k	k	σ_k
1	0.025		
2	0.077	1	0.007
3	0.132		
4	0.193		
5	0.260	2	0.260
6	0.334		
7	0.414		
8	0.500	3	0.500
9	0.588		
10	0.678		
11	0.765	4	0.765
12	0.845		
13	0.914		
14	0.967	5	0.967
15	0.996		

Table 1

Vertical resolution used in the experiments.

4. EVALUATION OF THE HIGH RESOLUTION SPECTRAL MODEL

Nine different 8-day prediction experiments have been carried out from the data set described above. Experiments have been carried out with spectral as well as gridpoint models. Table 2 specifies the different experiments. Both the gridpoint model as well as the very high resolution spectral models predict the actual weather events with remarkable accuracy. We will first describe the prediction with the highest spectral resolution. Fig. 4 and Fig. 5 show the RMS and correlation coefficient respectively for the whole of the troposphere (1000 - 200 mb) (verified for each standard level) and for the area to the north of 20 ^{o}N. The forecast has been verified in total as well as being de-composed in 3 different zonal wavenumber groups, ultra-long waves 1 - 3, medium long waves 4 - 9 and short waves 10 - 20.

Verification is done versus NMC's operational analysis and this means that there is initially a RMS difference of around 35 m. This is slightly higher than between two different analyses but the additional increase is most likely caused by vertical interpolation between σ - and p-surfaces and by the normal mode initialisation. The error growth is approximately linear with a doubling time of 5.5 days for the total field and almost 7 days for the long waves. Assuming an exponential growth gives a very similar doubling time. This particular weather situation is characterised by very large changes. Persistance reaches the norm between 1 or 2 days for all wave components. The large changes which occur during this weather situation are the reason why we obtain the very high correlation figures as can be seen from Fig. 5. The correlation for the long waves only drops from initially 0.95 to 0.80 after 8 days.

Notation	S60	T46	T45	T16	T15	T14	T17	R47	R66
Dataset	I	II	II	I	II	I	I	II	II*
Area of integration	global	global	global	global	N.H.	global	global	global	global
Horizontal resolution	P63/58/74	T63	T40	T40	T40	T21	T21	N48	N48
Vertical resolution	15	15	15	15	15	15	5	15	15
Parameterization Scheme	EC(b)	EC(b)	EC(b)	EC(a)	EC(b)	EC(b)	EC(a)	EC(b)	EC(b)

Table 2 : The table gives relevant information about 9 different prediction experiments. Two slightly different datasets have been used where the only difference between dataset I and dataset II is that in II satellite winds from GOES III (over the Indian Ocean) have been incorporated. It is not expected this will have noticeable influence on the experiments.
In II* all satellite data (temperatures and winds) have been excluded during the data assimilation. The 2 vertical resolutions used are given in Table 2.1 and the 2 different parameterization schemes EC(a) and EC(b) are presented in Table 8. P (pentagonal) and T (triangular) represent spectral resolution described in Figure 23. N represents grid point resolution described in the text.

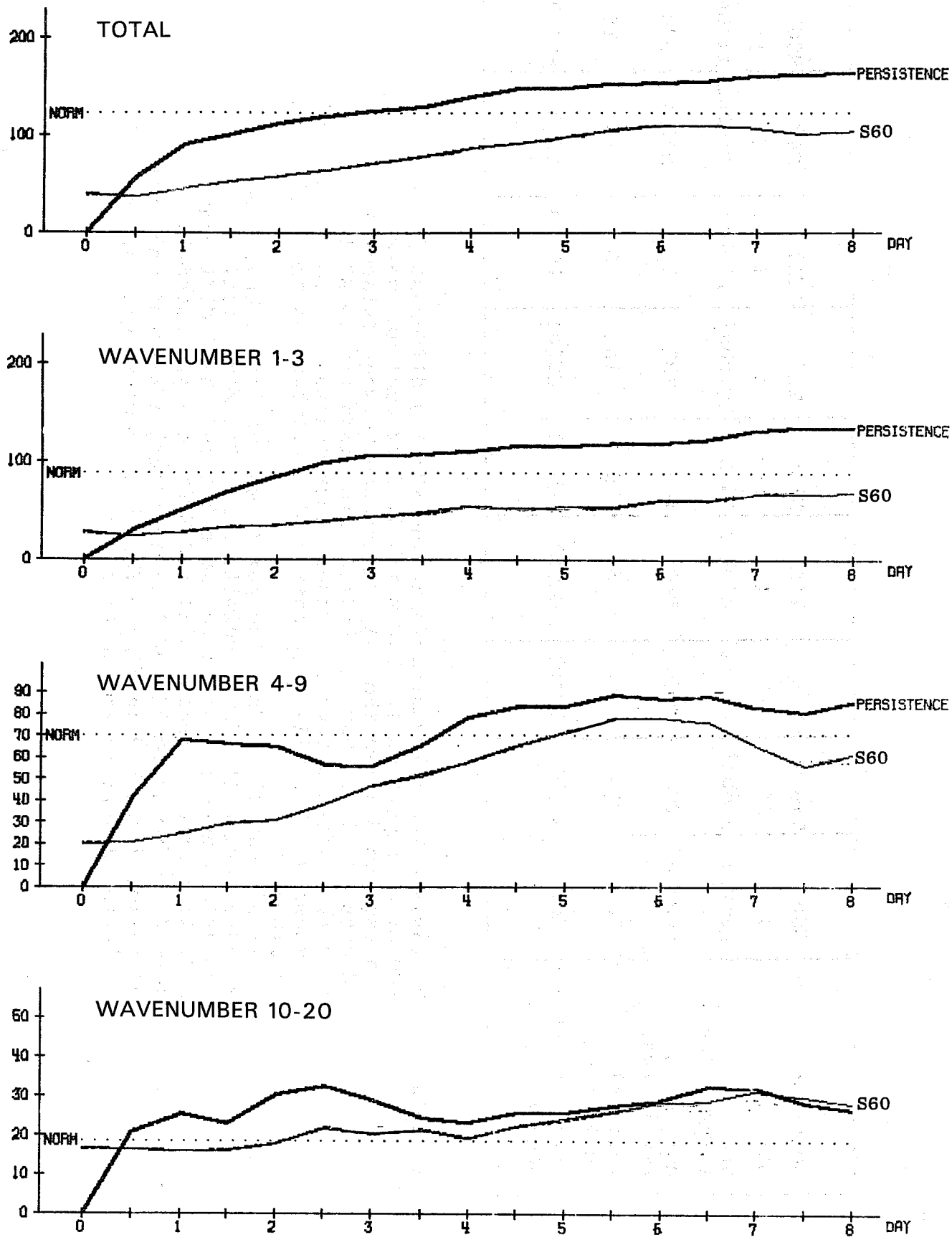

Fig. 4 Mean 1000 - 200 mb and 20.0 - 82.5 N RMS-error of height (M)

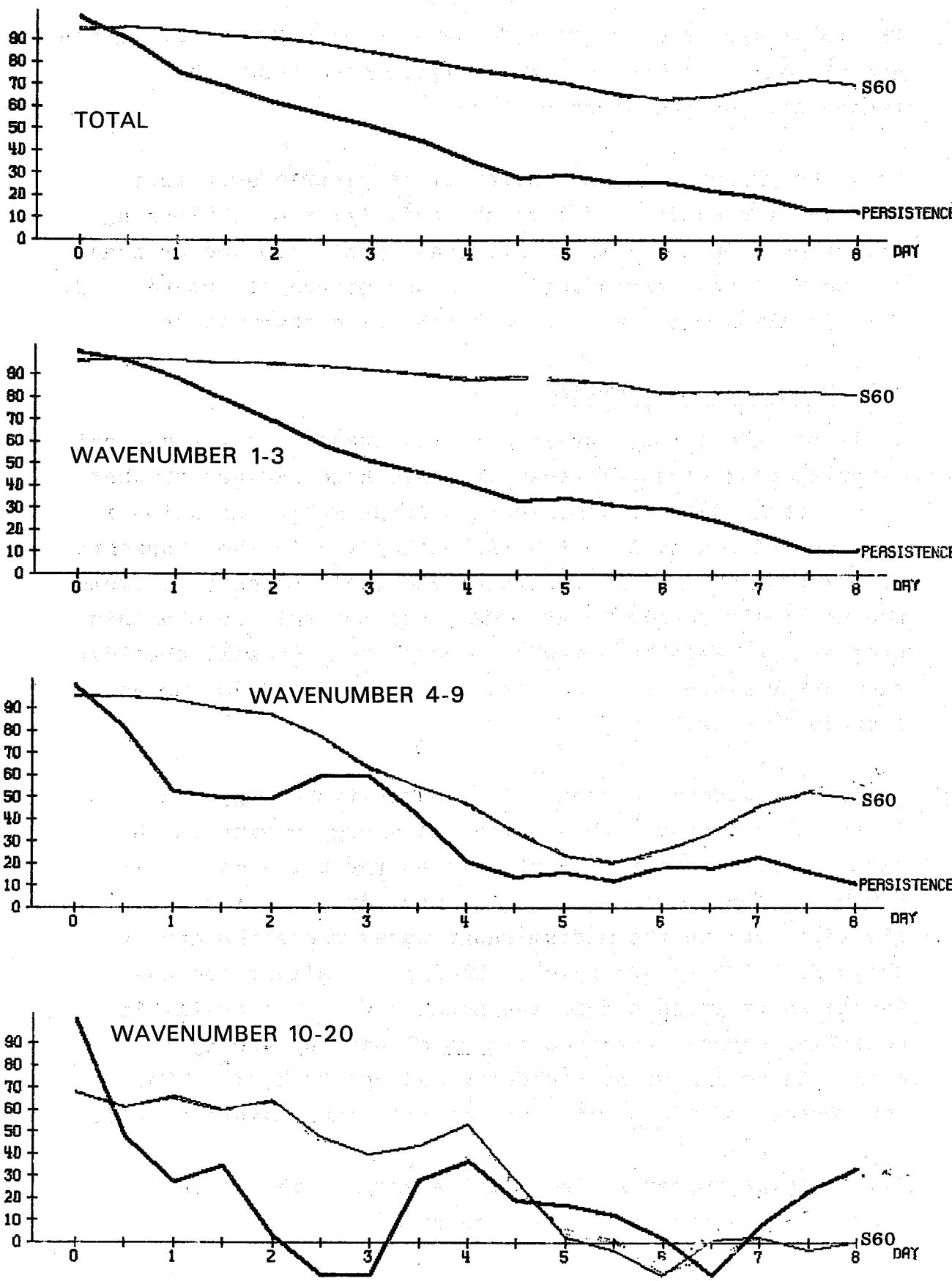

Fig. 5 Mean 1000 - 200 mb and 20.0 - 82.5 N Correlation of height %

The forecasts from 500 mb and corresponding NMC verification are presented in Fig. 6. This figure also shows the trajectory for the blocking high.

From the phenomenological point it is clearly seen that from day 4 onwards we fulfil the definition of a blocking situation. On day 8 the westerlies split into two branches around 70 W and merged again into one branch at around 10 E. This is almost in complete agreement with observations.

4.1 Diagnostic evaluation

It is of interest to investigate the changes in the general circulation during a forecast of this kind and see to what extent the model can describe the large scale variation in kinetic and available potential energy and in the transport of momentum and heat. Unfortunately the diagnostic systems are not fully developed at ECMWF, and for this reason this presentation will be somewhat incomplete. We will consider the energy diagnostics between the surface and 200 mb and from 20 ^{o}N - 82.5 ^{o}N.

There is a general decrease in the kinetic energy and increase in the available potential energy during the 8 days. The reduction in kinetic energy falls mainly in the ultra long waves where the energy drops from 850 to 480 kj/m^2 and in the medium range waves where the energy drops from 560 to 430 kj/m^2. There is a slight increase in the short waves and in the zonal part. The available potential energy increases its zonal part by 400 kj/m^2 while the medium waves are decreased by 130 kj/m^2. The long waves and the short waves do not change significantly.

By and large therefore the total energy is therefore approximately conserved over the area.

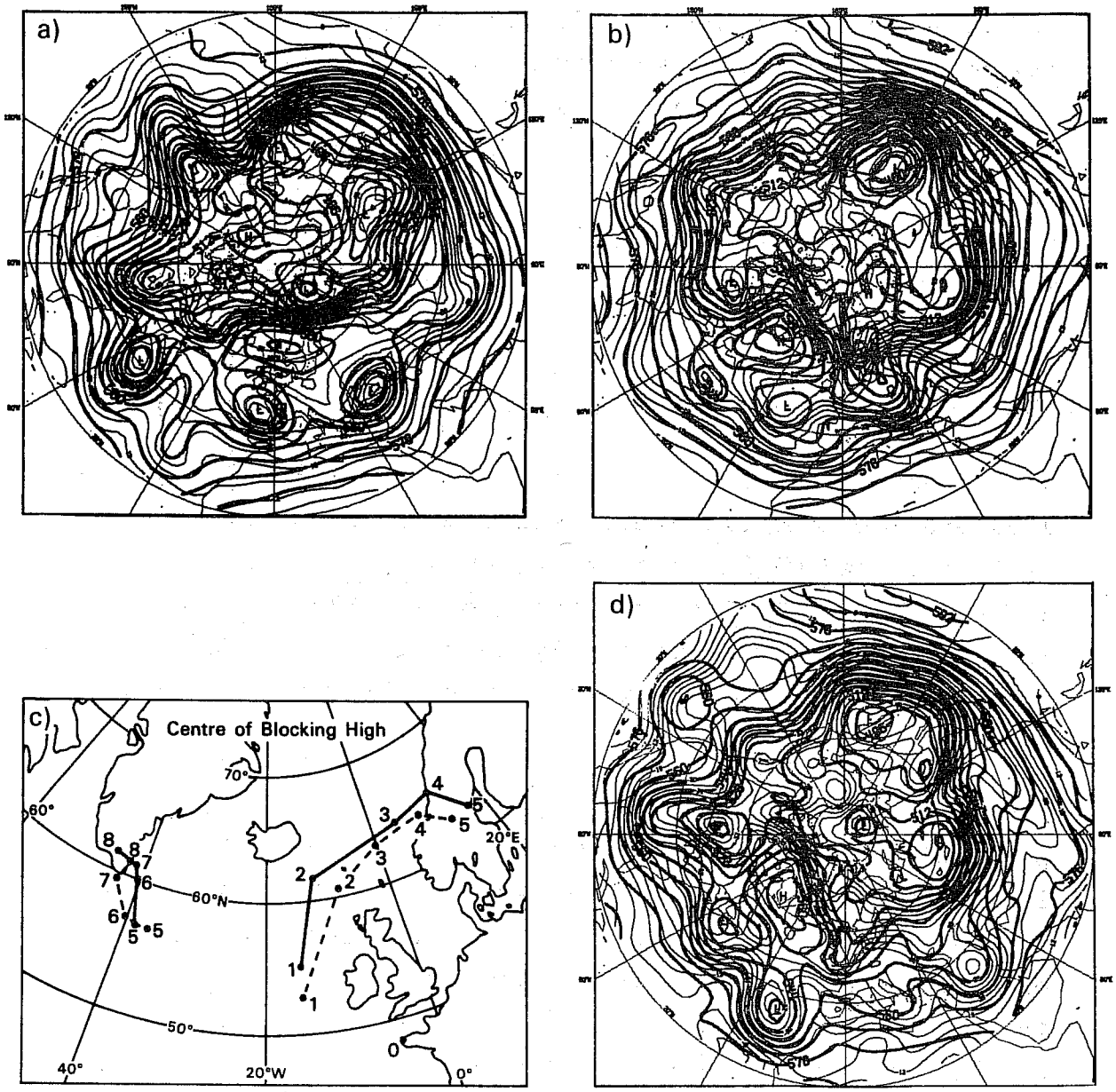

Fig. 6 500 mb geopotential (full lines) and temperatures (thin lines) for (a) 4 day forecast with the high resolution spectral model, S 60, (b) 8 day forecast, (c) full lines observed trajectories for the blocking high day by day, dashed lines predicted trajectories day by day, (d) observed 500 mb at 24/1 00Z.

The high resolution model, S60, predicts these changes rather well, as can be seen from Fig. 7 and Fig. 8. In general there is a slight loss in kinetic energy, in particular for the short waves. It is also clear that S60 reduces the available potential energy of the ultra long waves by as much as 200 kj/m^2, where in fact the energy in reality does not drop at all. The underestimation of kinetic energy mainly takes place around the jet stream, while there is a slight tendency to an overestimation in the lowest part of the atmosphere.

The transfer of available potential energy between the zonal flow and the long and medium scale waves respectively is well predicted with a mean transfer $A_{zonal} \rightarrow A_{eddy}$ of 1.6 - 2 Wm^{-2} to each of the two groups. The transfer to the short waves is subtantially less, 0.2 - 0.4 Wm^{-2}. Fig. 9 shows a good agreement between observation and prediction.

A vertical cross-section for the zonal wind for the predication and the observed values is shown in Fig. 10. This figure shows the mean values for the first 4 days as well as for the last 4 days. It can be seen that the easterly winds in the lower troposphere from the first to the second period extend from 75 ^{o}N to 55 ^{o}N. On average we therefore have easterly winds over the whole hemisphere north of 55 ^{o}N during the second 4-day period. Fig. 11 shows the corresponding error in the zonal wind. During the first 4 days the error is very small and of relatively small scale. During the second 4-day period, however, a more well-defined error pattern appears. We can there see that the forecast overestimates the easterly winds at high latitudes. The forecast also underestimates the intensity of the subtropical jet and also moves the centre of the jet too far to the north. This error has been reduced in a later version of the model by introducing a more realistic parameterisation of the Kuo convective scheme.

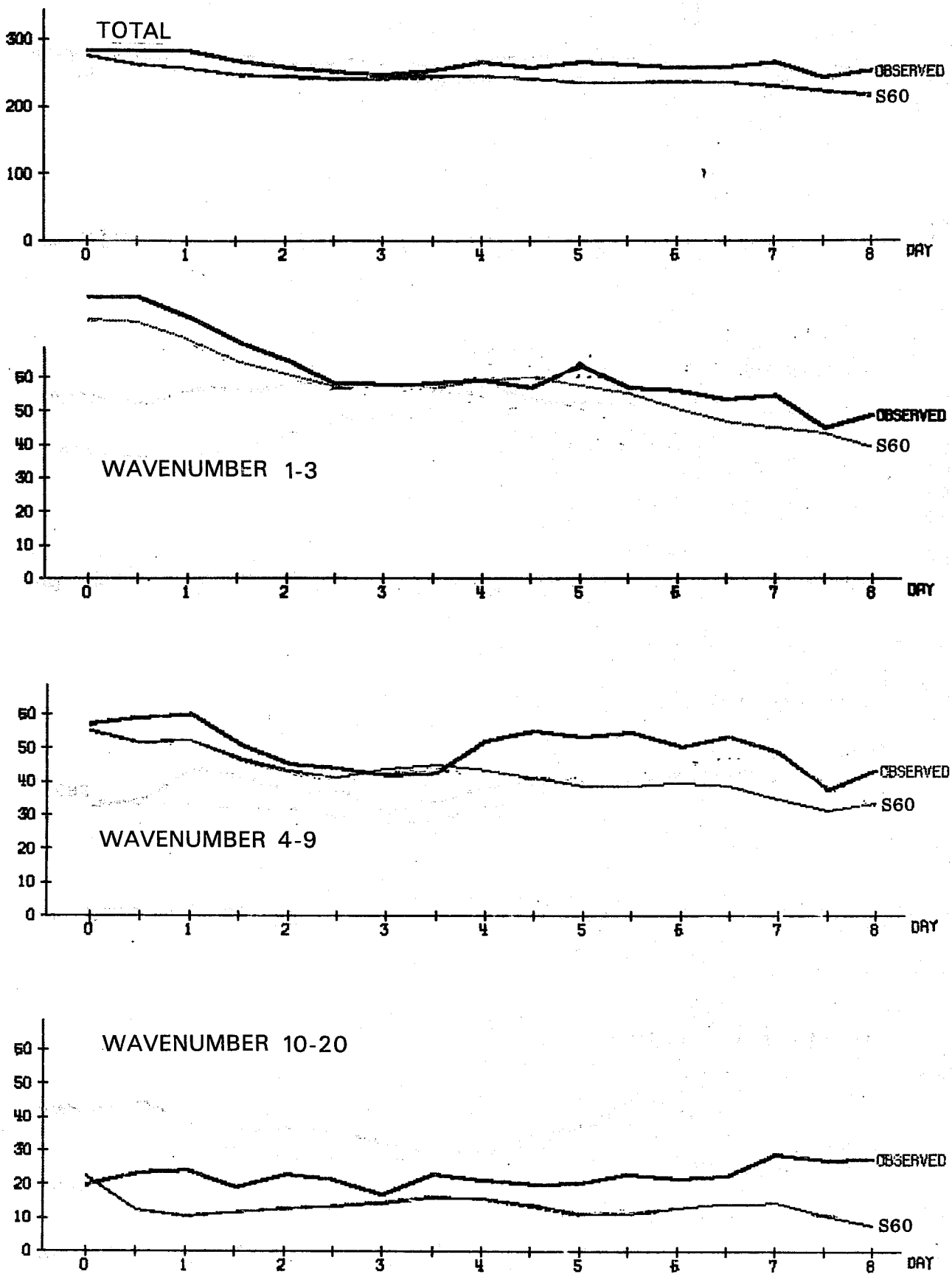

Fig. 7 Kinetic energy (geostrophic) as a function of time. Heavy line observed, thin line predicted. The kinetic energy has been averaged for the levels 1000 - 200 mb and for the area 20^{o}N - 82.5^{o}N. Unit 10 JK/m^2.

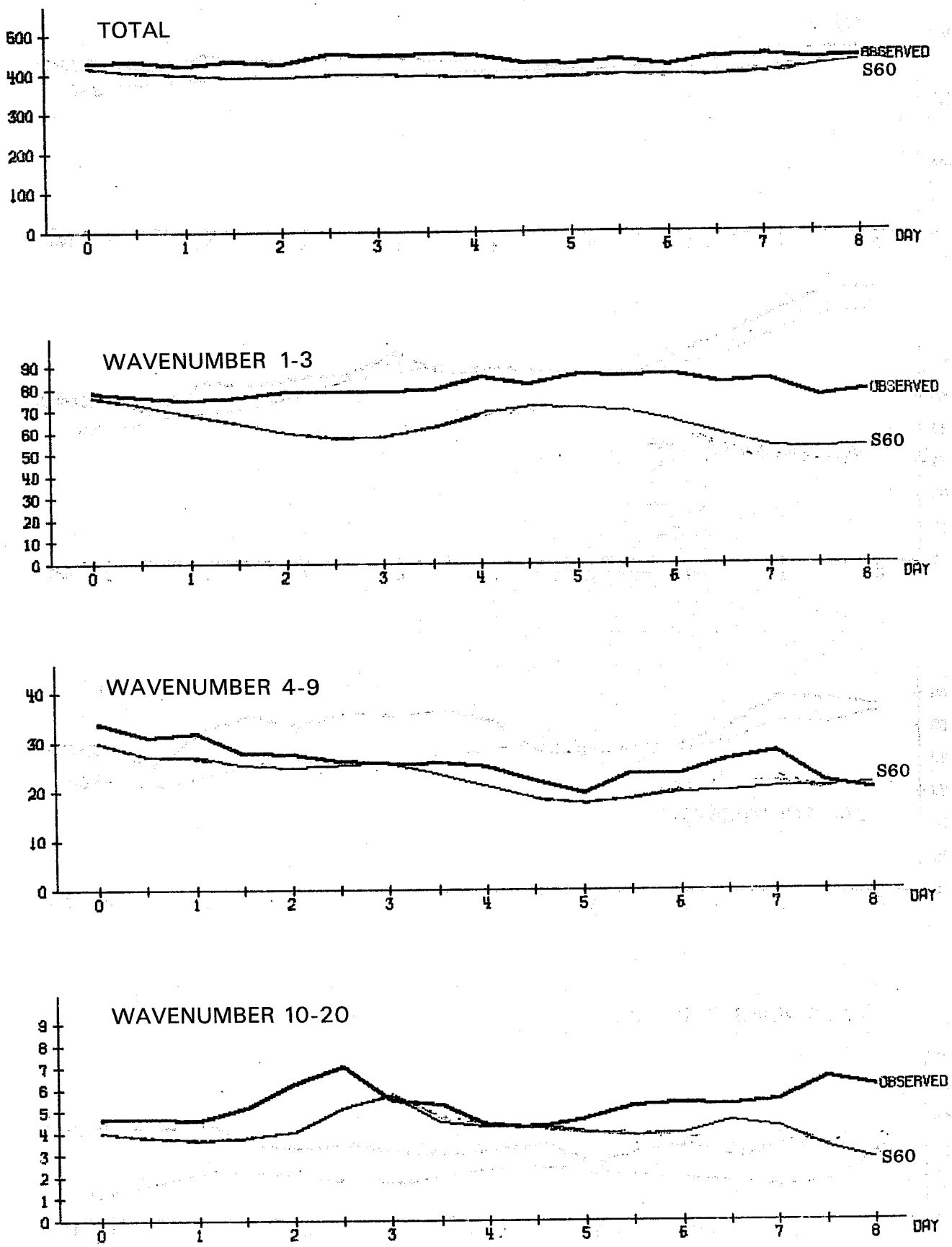

Fig. 8 Available potential energy as a function of time. Heavy line observed, thin line predicted. The available potential energy has been averaged for the levels 850 - 200 mb and for the area $20^{o}N$ - $82.5^{o}N$. Unit 10 KJ/m^2.

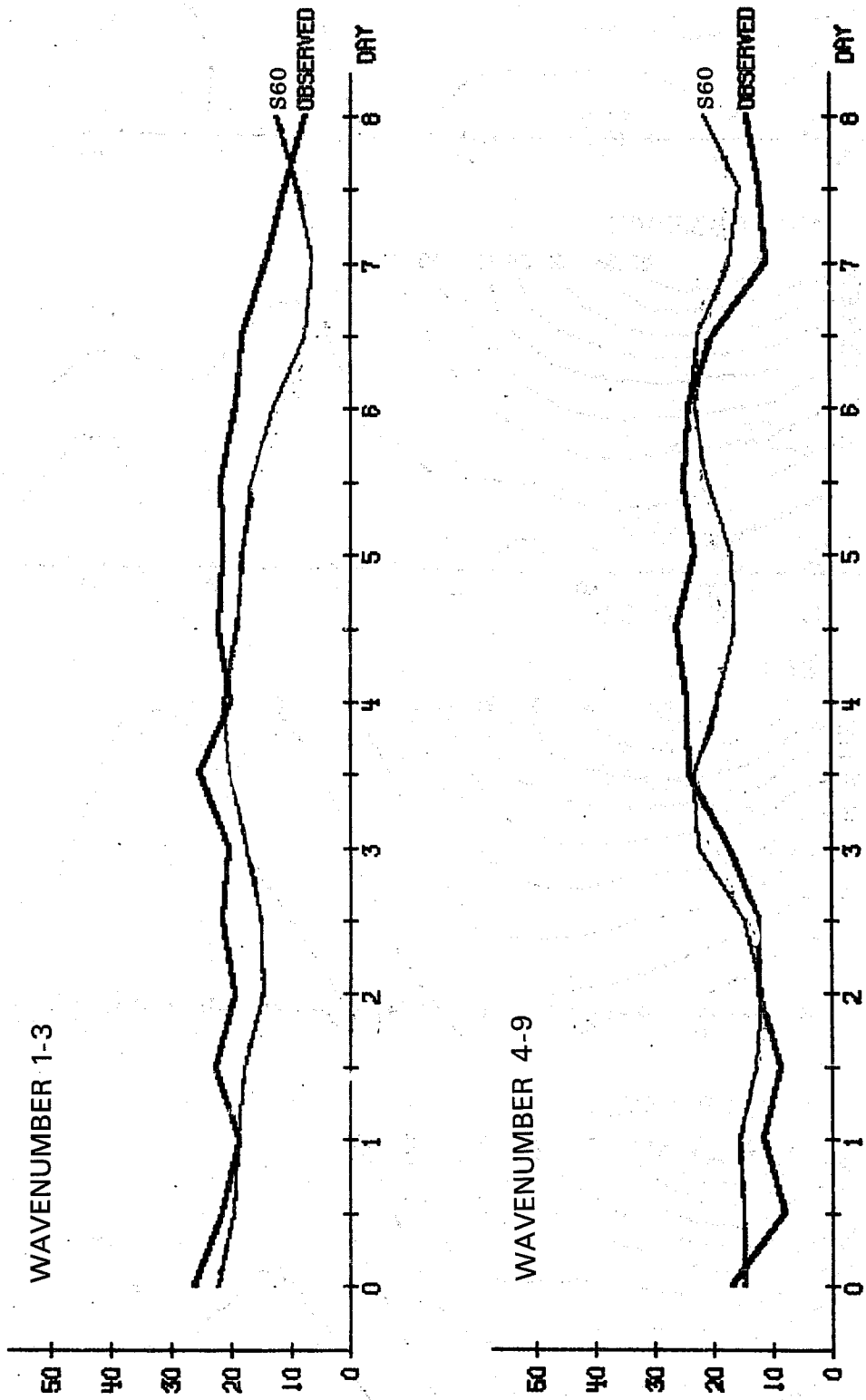

Fig. 9 Conversion between zonal and eddy available potential energy as a function of time. Heavy line observed, thin line predicted. Positive values means conversion from the zonal part to the eddy part. The conversion has been averaged for the levels 850 - 200 mb and for the area 20^{o} N - 82.5^{o} N. Unit 10^{-1} KJ/m^2.

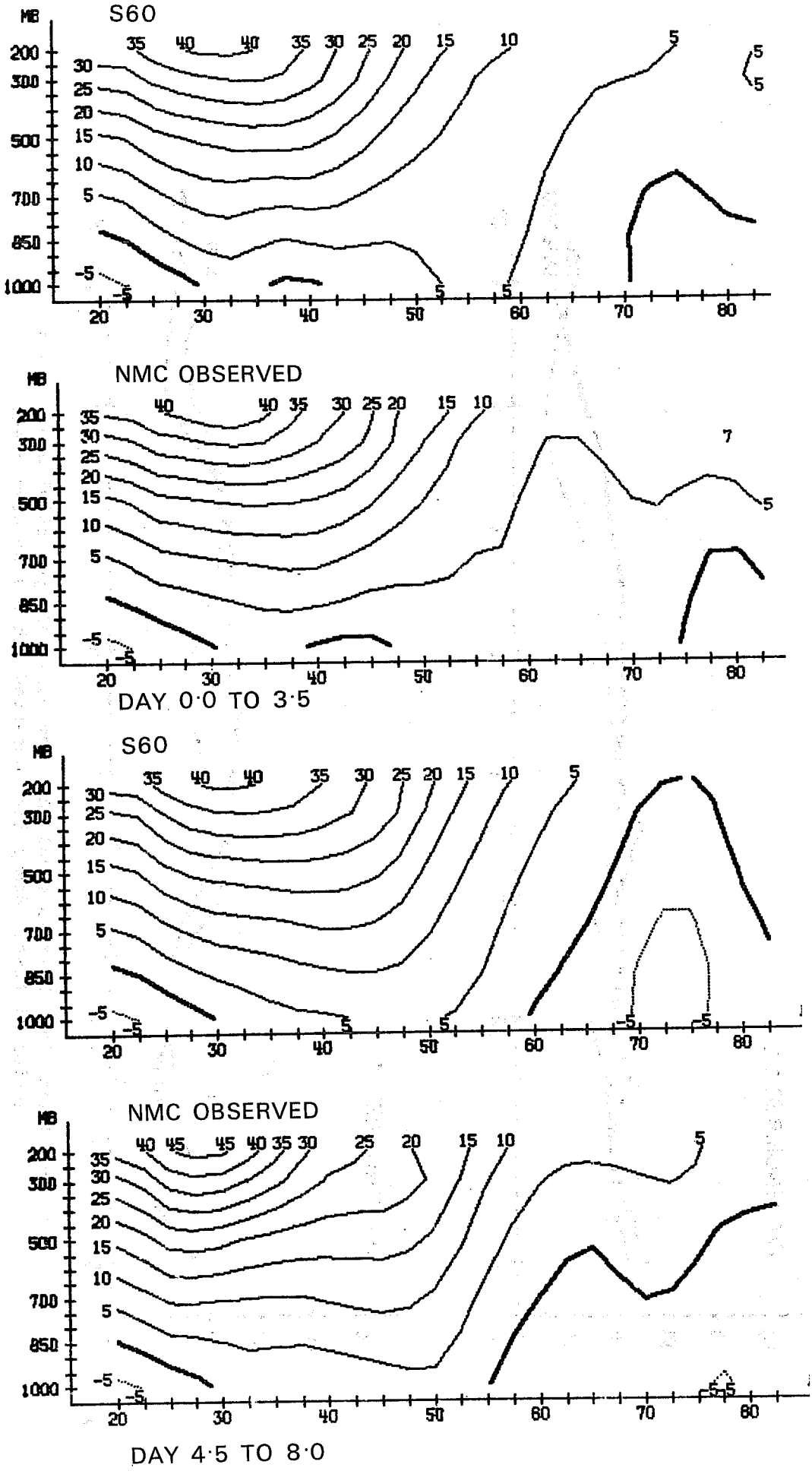

Fig. 10 Vertical cross section of predicted and observed zonal wind. Upper part gives the average for the first 4 days and the lower part the average for the second 4 days. Unit m/sec.

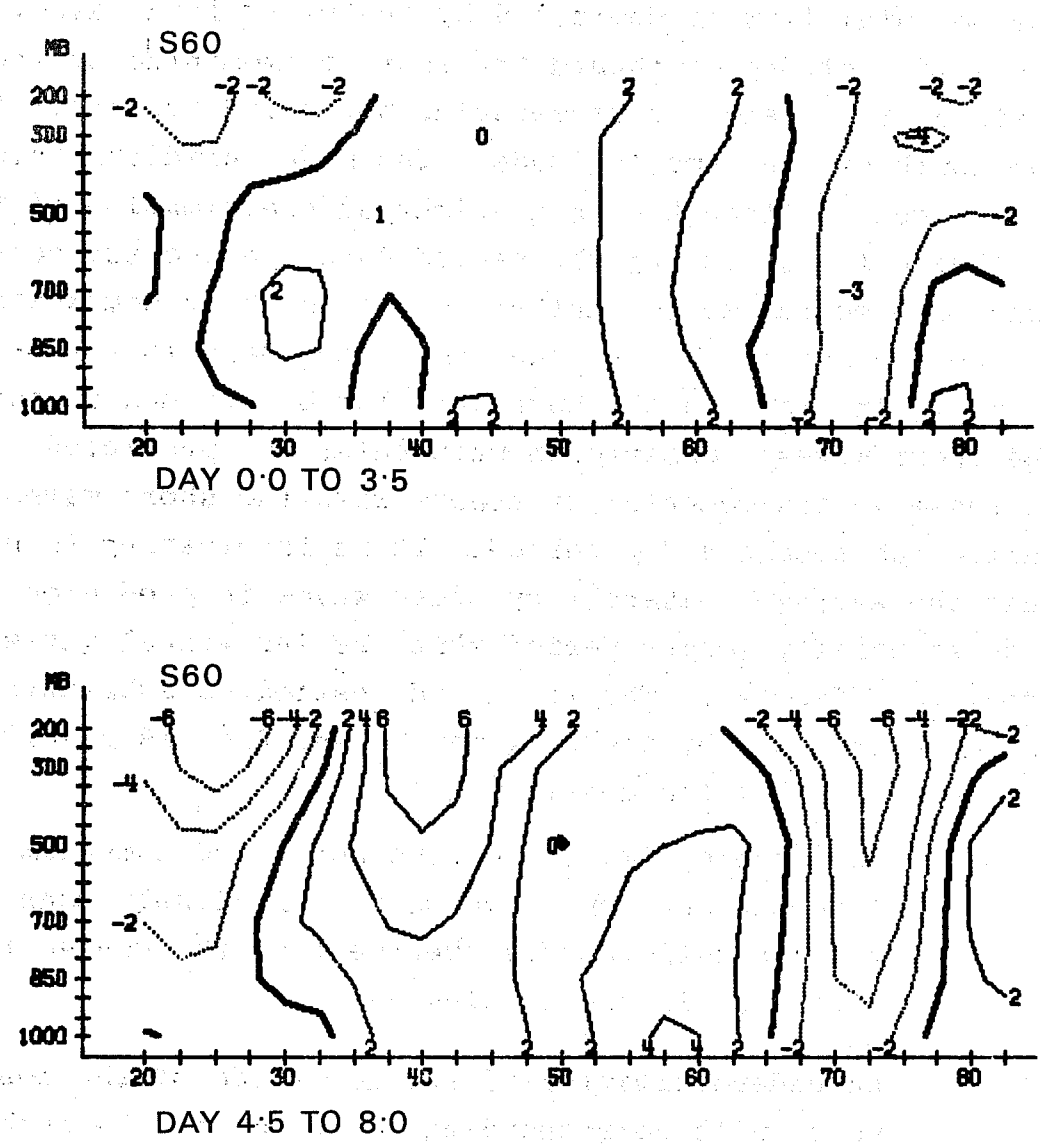

Fig. 11 Vertical cross section of the prediction error of the zonal wind, $U^{pred} - U^{obs}$. Upper part gives the average error for the first 4 days and the lower part the average for the second 4 days. Unit m/sec.

The observed and predicted momentum flux is shown in Figs. 12, 13, and 14 for the three groups of wave lengths and as mean values for the two 4-day periods. During the first 4 days the momentum flux is dominated by the ultra long waves. There is a strong southward transport of momentum to the north of 55 ^{o}N and a corresponding northward transport to the south of the same latitude. The model predicts this rather well, although with a slight underestimation of the southward flux. During the second 4-day period the convergence of momentum moves further to the south to somewhere between 40 and 50 ^{o}N. At the same time there is a substantial increase in the momentum-flux by the medium and the short waves. Observe in particular the predicted increase in the momentum transport with the short waves during the second 4-day period. It is interesting to note that the average transport by these waves is predicted for a substantially longer period than the individual waves are predicted (Fig. 4). The model underestimates substantially the momentum flux by the long waves, and Fig. 19 highlights two weaknesses of the model, namely

(i) the underestimation of the northward momentum flux from the subtropics which is very likely connected to an unsatisfactory treatment of the convective processes in the tropics and

(ii) an underestimation of the amplitude of the long waves with corresponding reduction in the capacity of the transporting momentum.

The prediction of temperature is better than the momentum forecasts and only a slight cooling tendency can be seen in the upper troposphere, Fig. 15. The transport of sensible heat is also more satisfactory, Figs. 16 and 17. Observe the dual maximum during the first 4 days. The only substantial difference during the second period is that the long waves have their maximum transport around 8^{o} to the north compared with the observed states. The transport of sensible heat with the short waves is insignificant.

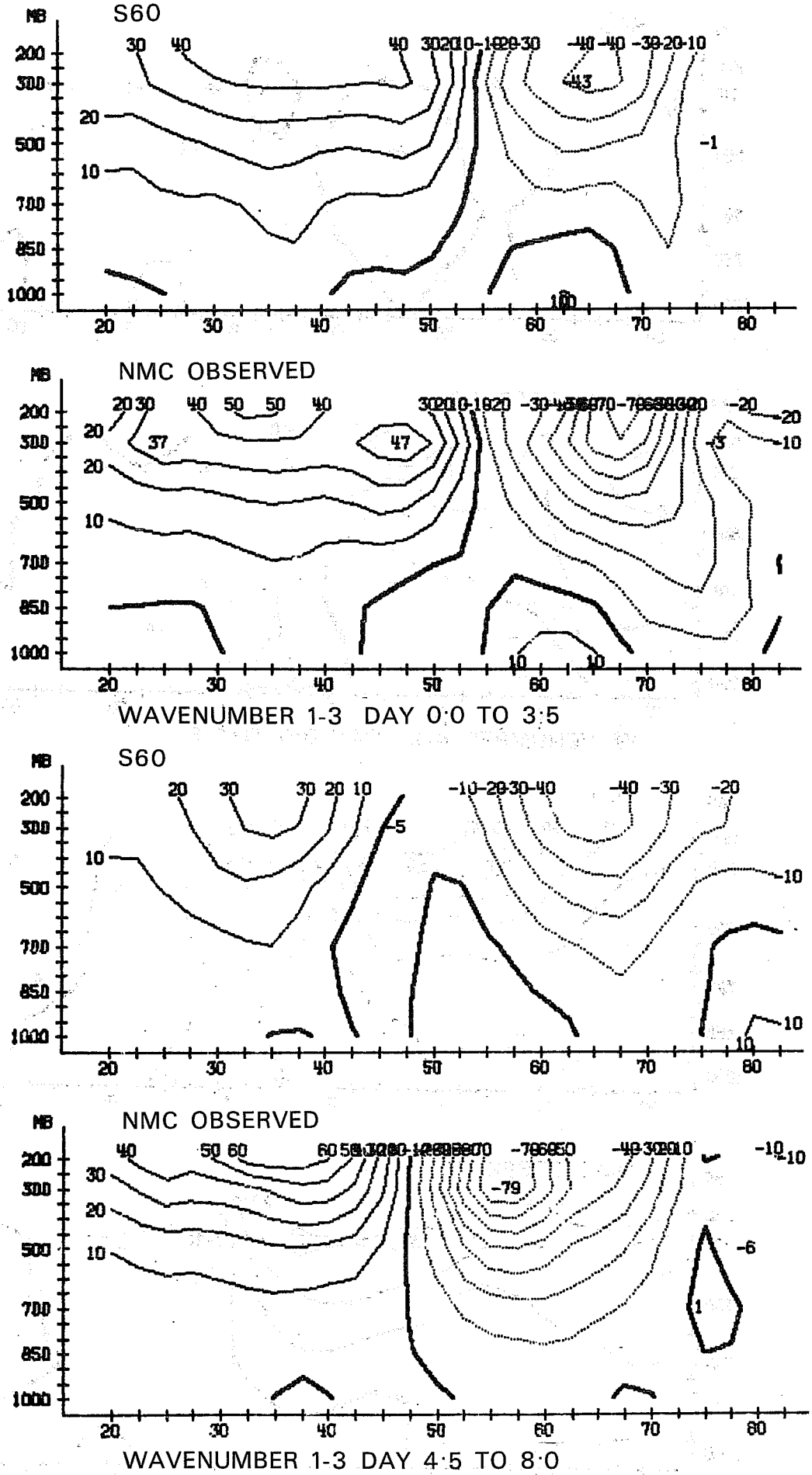

Fig. 12 Vertical cross section of predicted and observed momentum flux calculated from the geostrophic wind. Positive values northward momentum transport, negative values southward momentum transport. Upper part gives the average for the first 4 days and the lower part the average for the second 4 days. Unit $m^2/(sec)^2$.

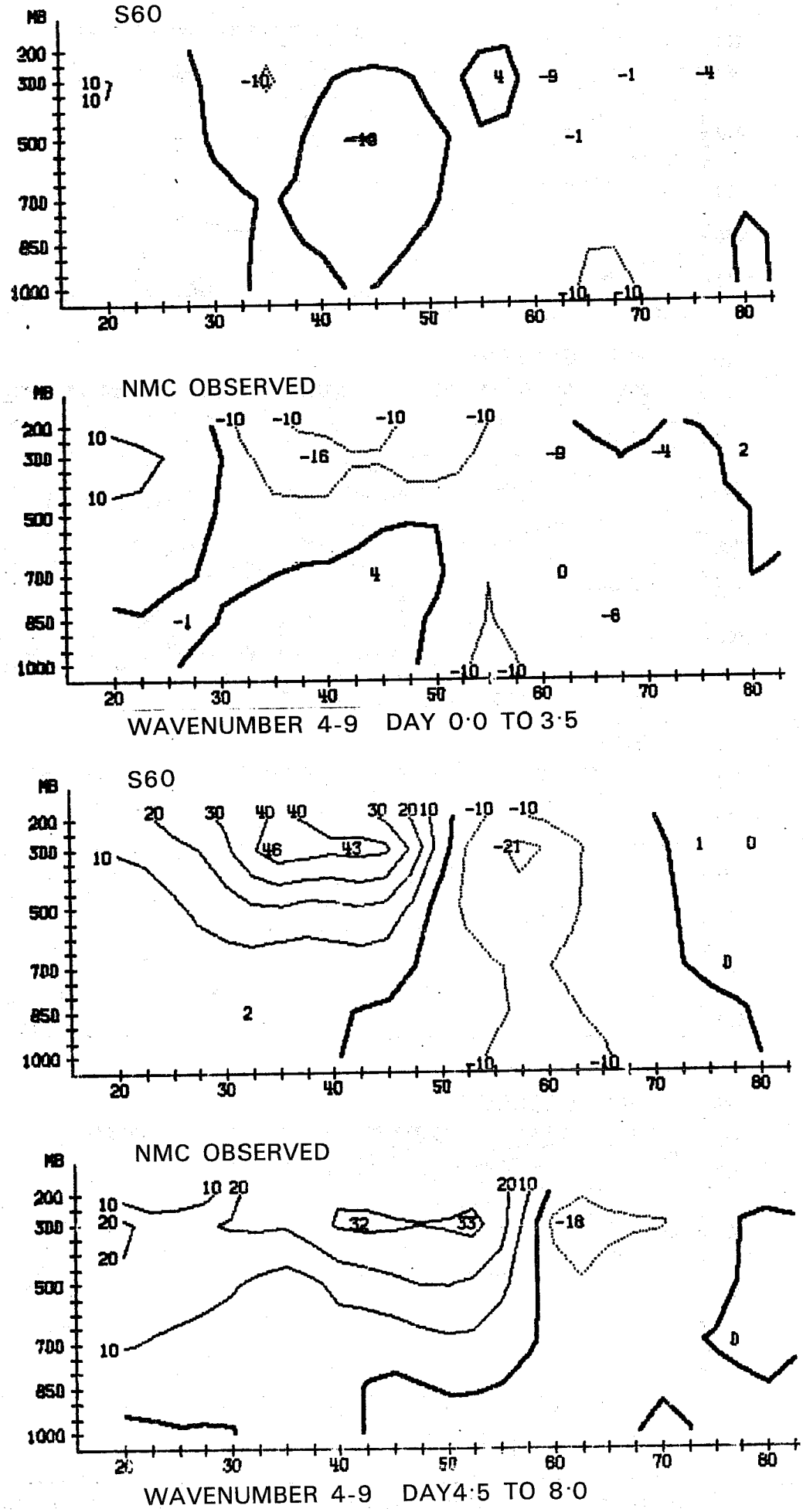

Fig. 13 The same as Fig. 12 but for wavenumber 4 - 9.

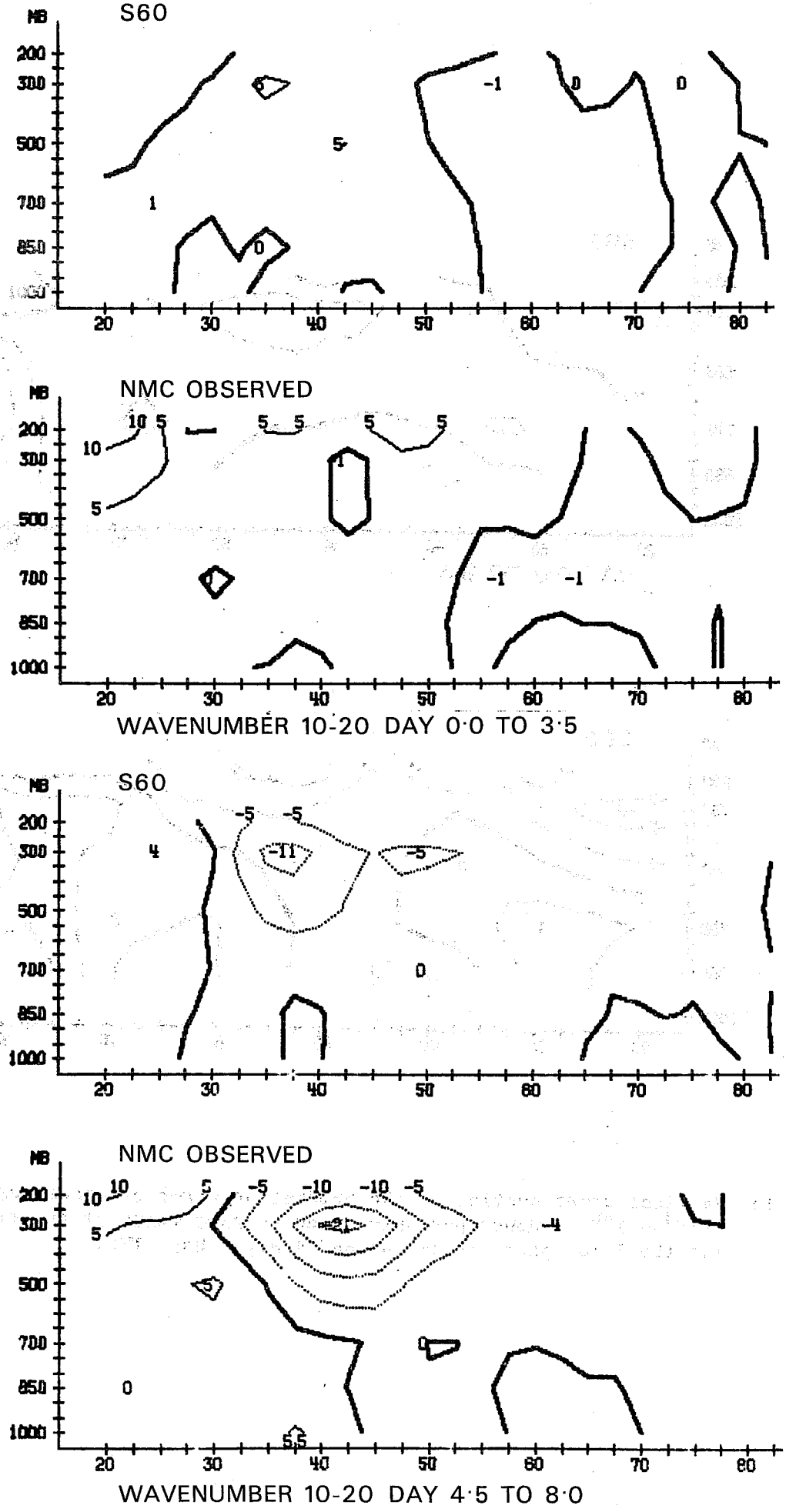

Fig. 14 The same as Fig. 12 but for wavenumber 10-20.

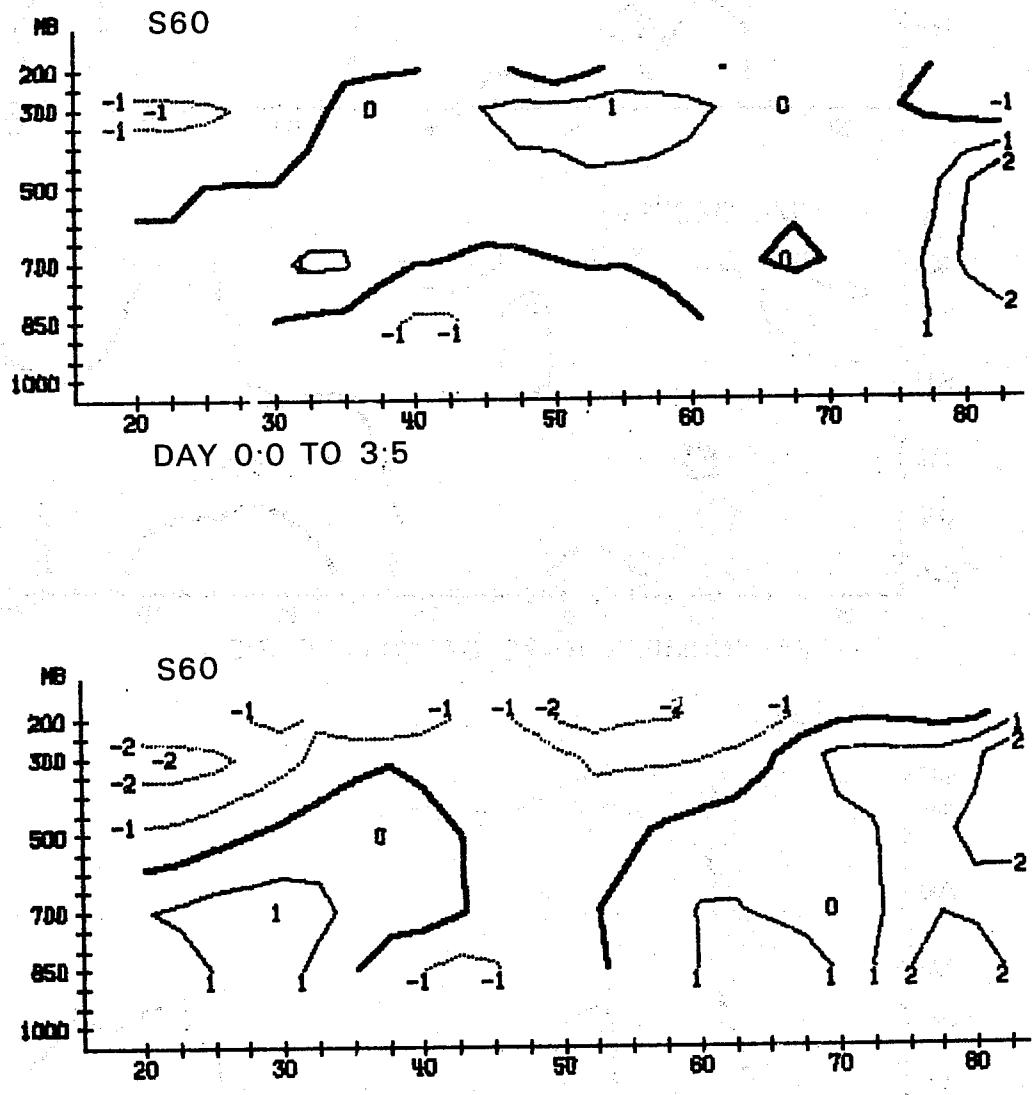

Fig. 15 Vertical cross section of the prediction error of zonal temperature, $T^{pred} - T^{obs}$. Upper part gives the average value of the first 4 days and the lower part for the second 4 days. Unit $T^{o}C$.

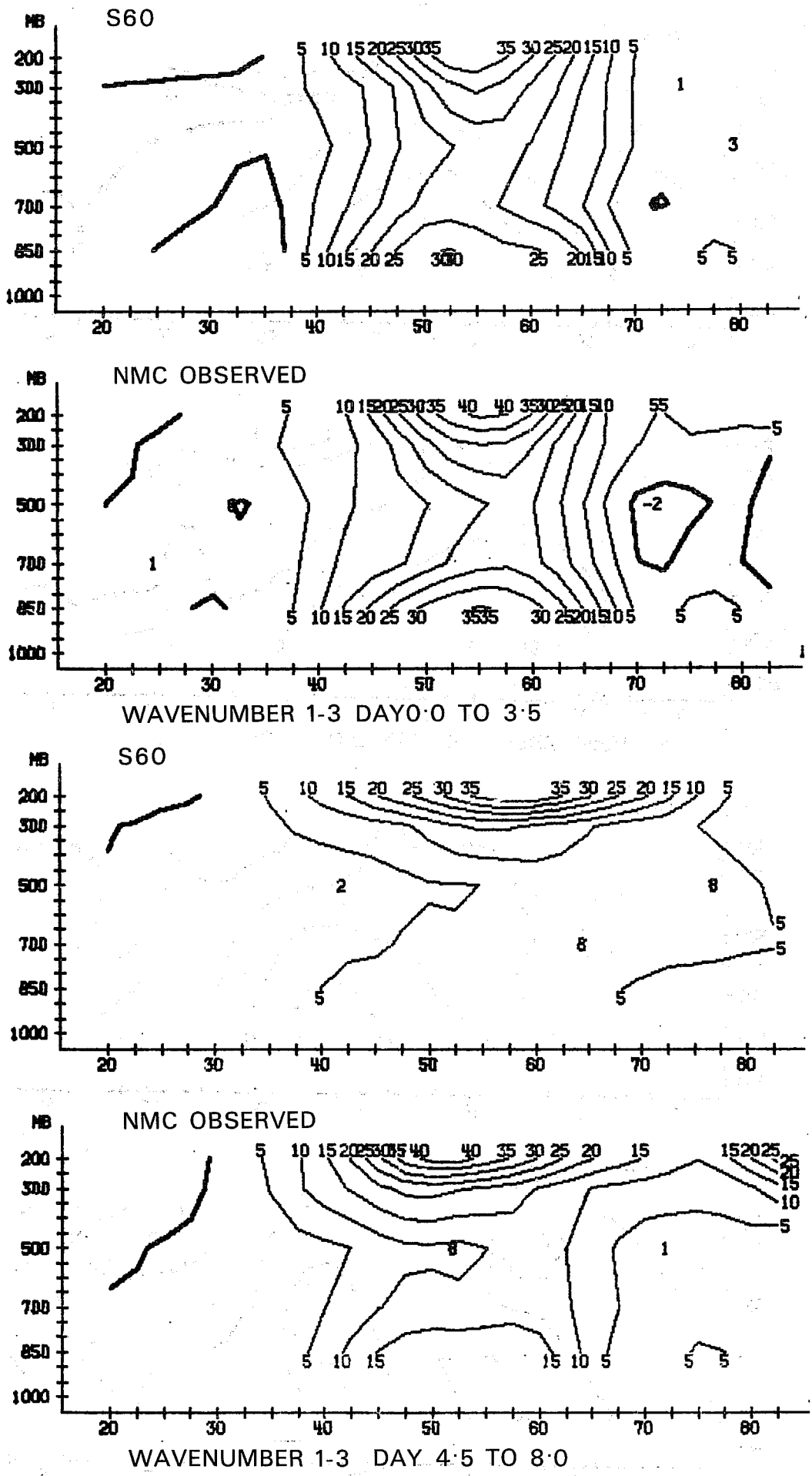

Fig. 16 Vertical cross section of predicted and observed sensible heat flux for wavenumber 1 - 3 and calculated from the geostrophic wind. Positive values northward transport. Upper part gives the average for the first 4 days and the lower part the average for the second 4 days. Unit ^{o}KM/sec.

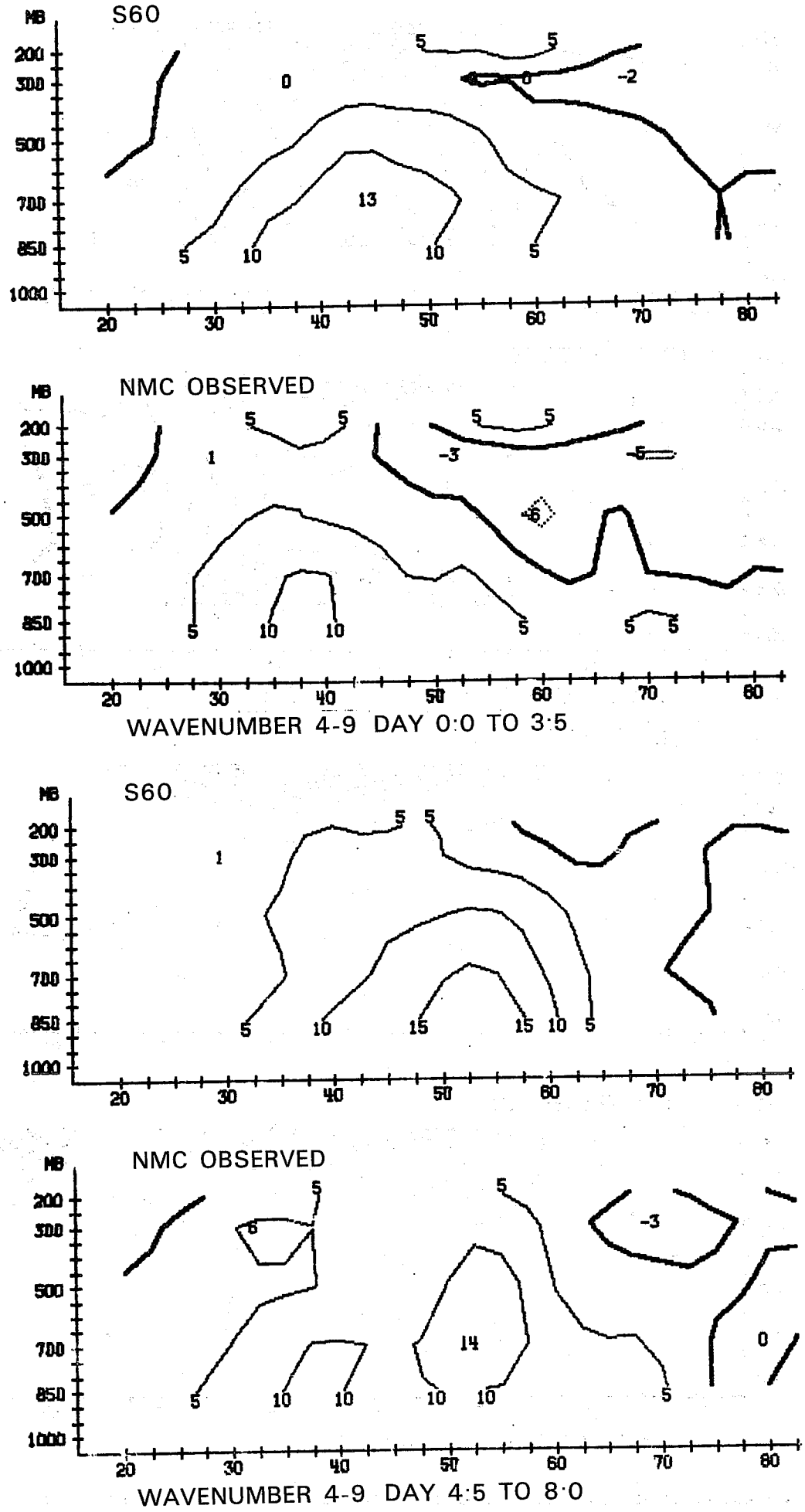

Fig. 17 The same as Fig. 16 but for wavenumber 4 - 9.

The reason that we have a satisfactory transport of sensible heat with the long waves in spite of an underestimation of the amplitude must be due to the fact that these waves are predicted to have a somewhat larger tilt through the troposphere.

A very detailed evaluation of the phase and amplitude prediction of individual waves and groups of waves shows nothing of particular interest. Figs. 18 and 19 show the Hovmöller diagram for the ultra long waves for the geopotential at 500 mb and temperature at 850 mb. The agreement with observations is very good. Harmonic dials giving phases and amplitudes have also been calculated for the largest spherical harmonic coefficients. Wave components M=1, N=1 in Fig. 20, wave component M=1, N=3 in Fig. 21 and wave component M=1, N=5 in Fig. 22 show that the ultra long waves are very well predicted.

5. RESULTS FROM OTHER MODELS

We will now go through an exercise where we successively will simplify the high resolution model and investigate to what extent this will reduce predictability in general and the predictability of the blocking episode in particular.

We will investigate the predictability in this case as a function of

(i) resolution
(ii) the integration domain
(iii) the parameterisation
(iv) the initial data.

Finally we will briefly comment on the predictability of some very simple models.

The different experiments are summarised in Table 2.

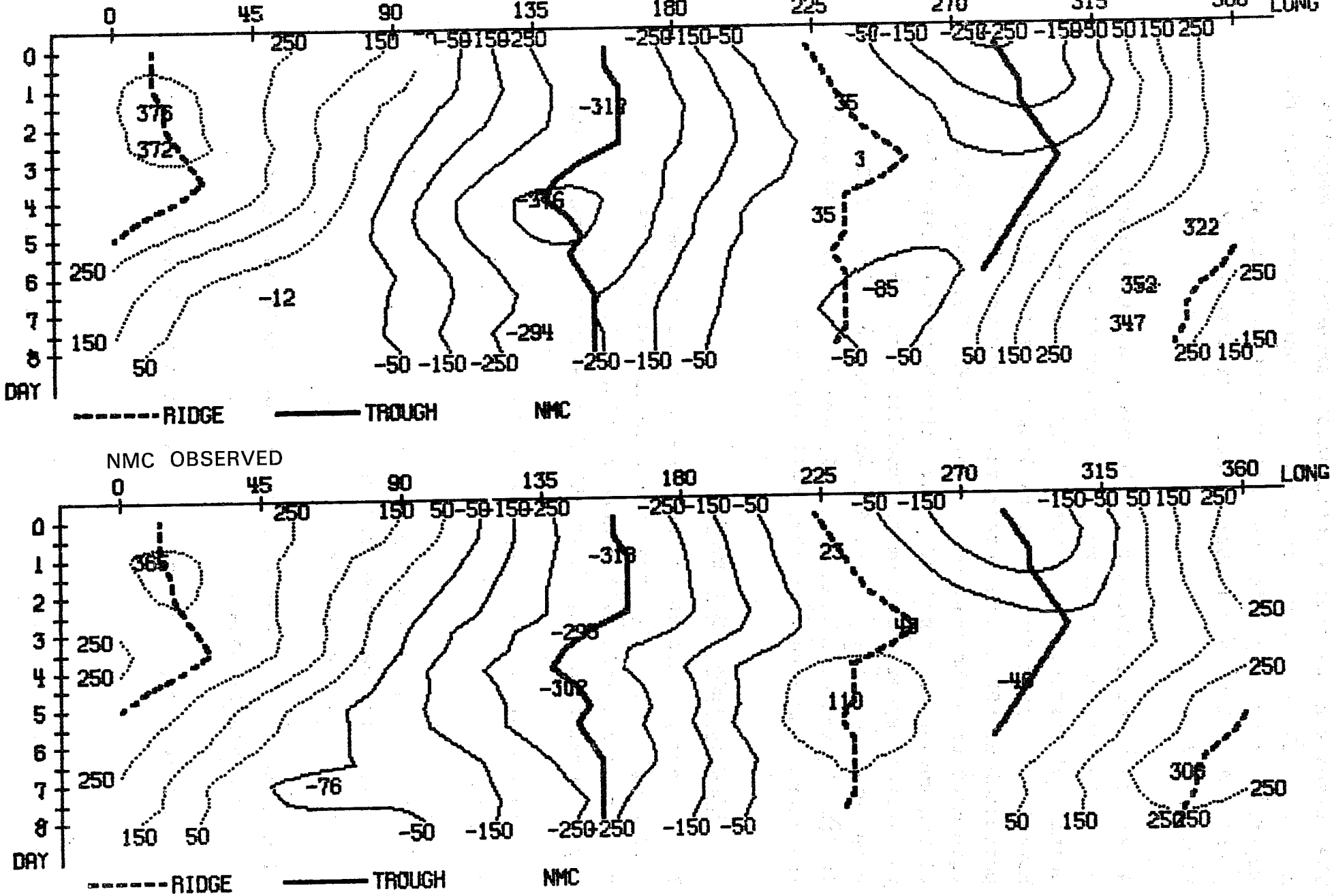

Fig. 18 Hovmöller diagram for predicted and observed long waves for 500 mb geopotential height. Full heavy lines observed trough lines, dashed heavy lines observed ridge lines.

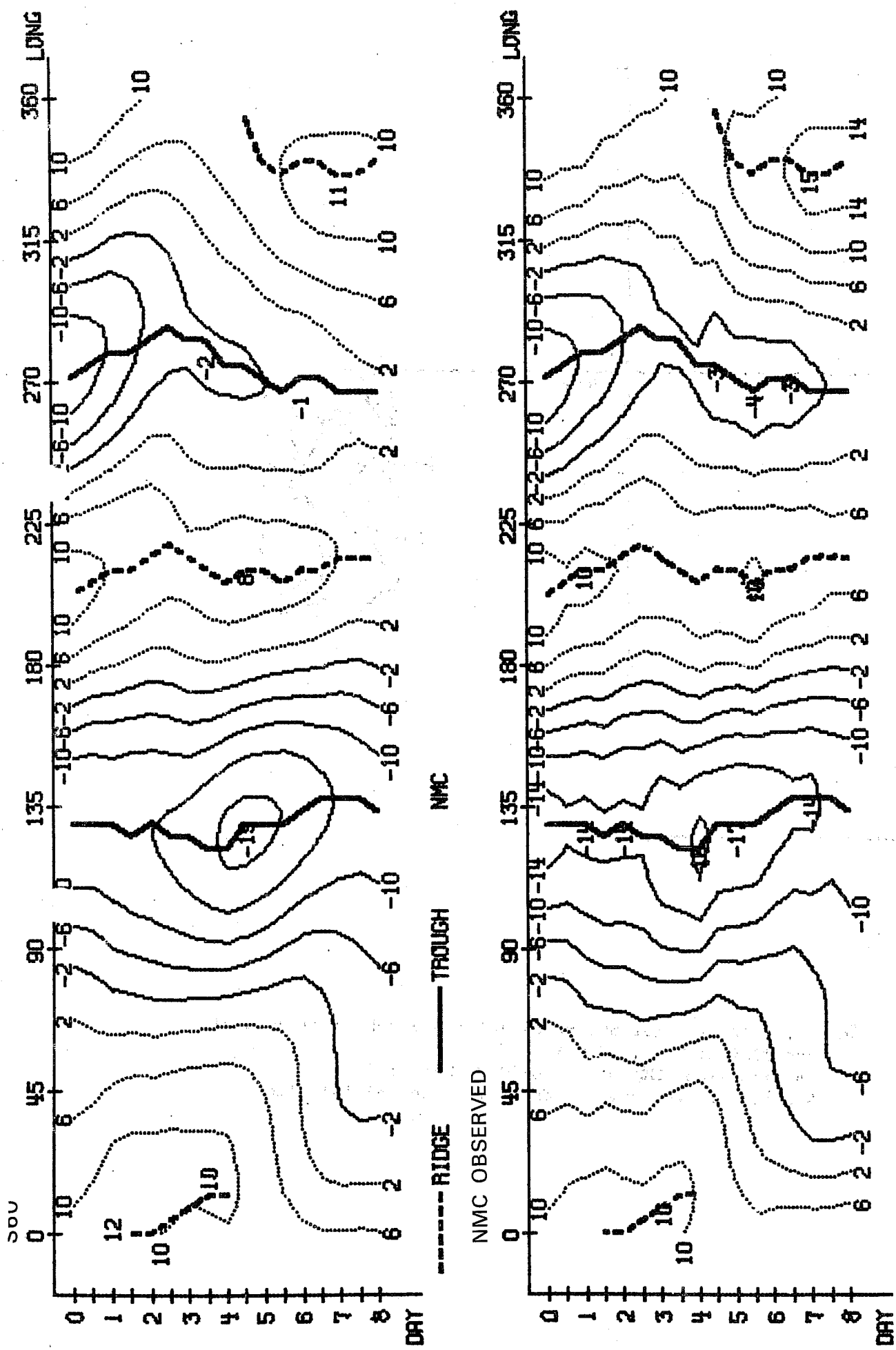

Fig. 19 Hovmöller diagram for predicted and observed long waves for 850 mb temperature. Full heavy lines observed temperature trough lines, dashed heavy lines observed ridge lines.

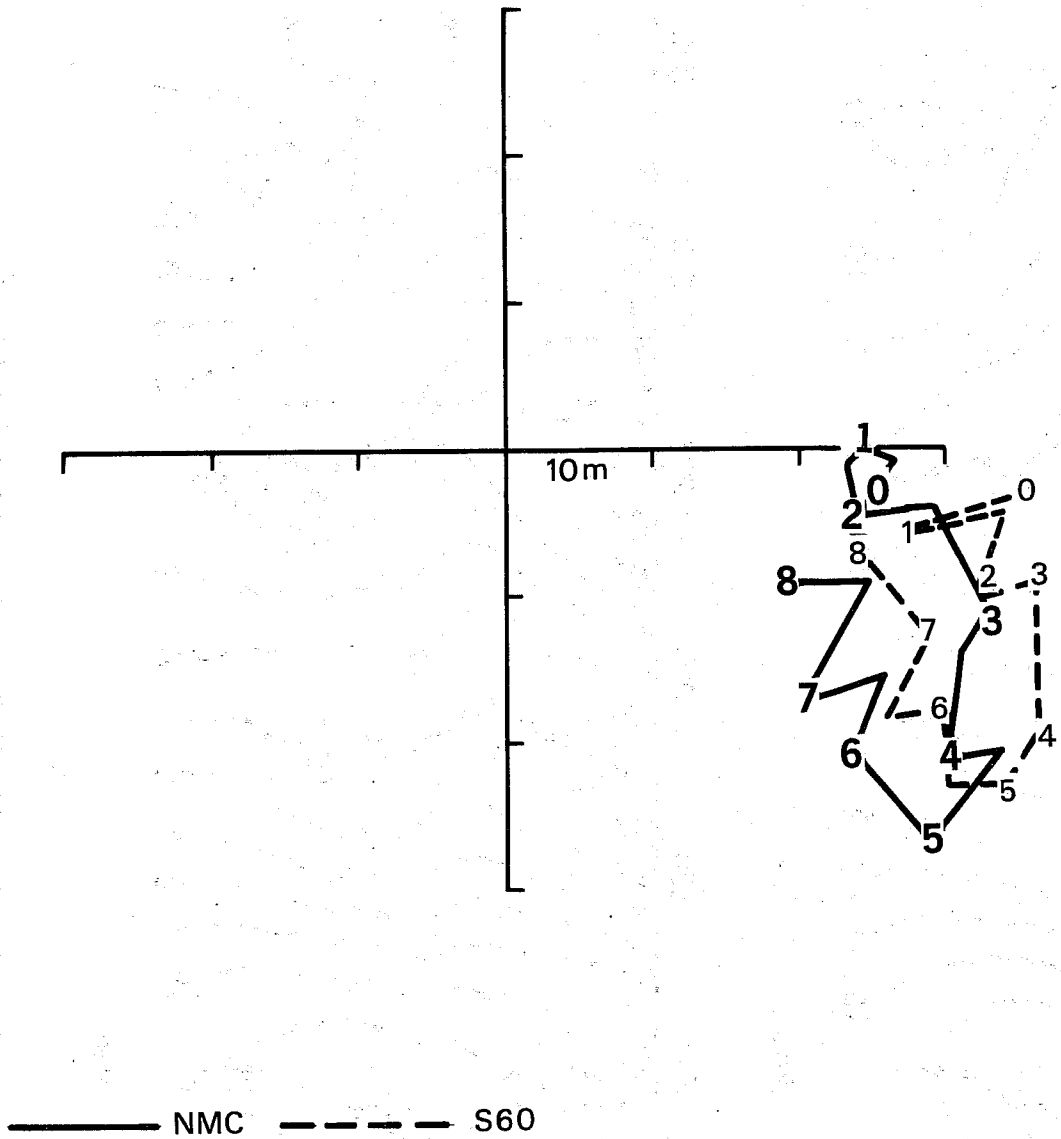

Fig. 20 Harmonic dial for 500 mb height field spherical harmonic coefficient M = 1, N = 1
Initial time (Day 0) : 79011600, Unit : 10 M
Numbers are the time in days from the initial time

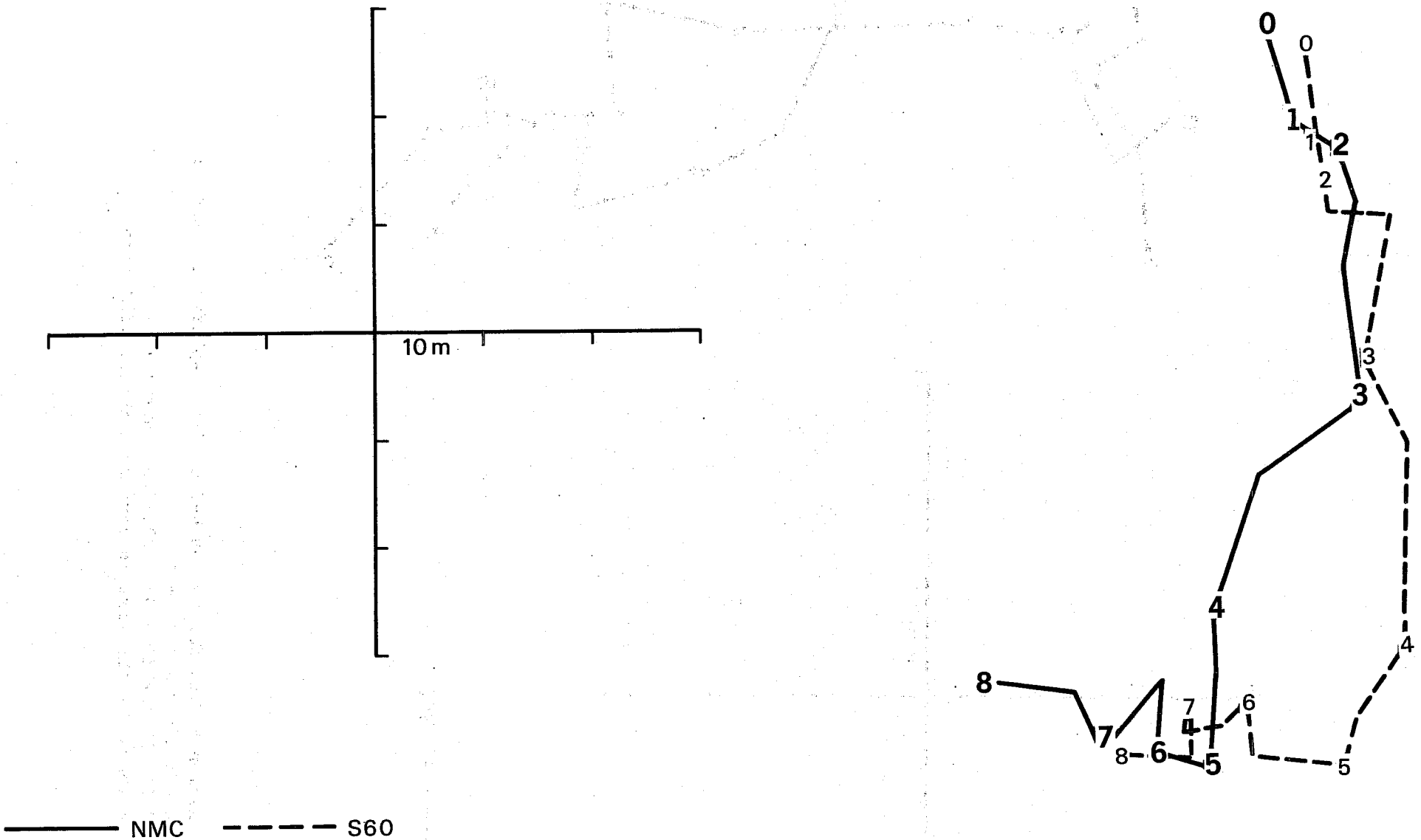

Fig. 21 Harmonic dial for 500 mb height field spherical harmonic coefficient M = 1, N = 3
Initial time (Day 0): 79011600, Unit : 10 M
Numbers are the time in days from the initial time

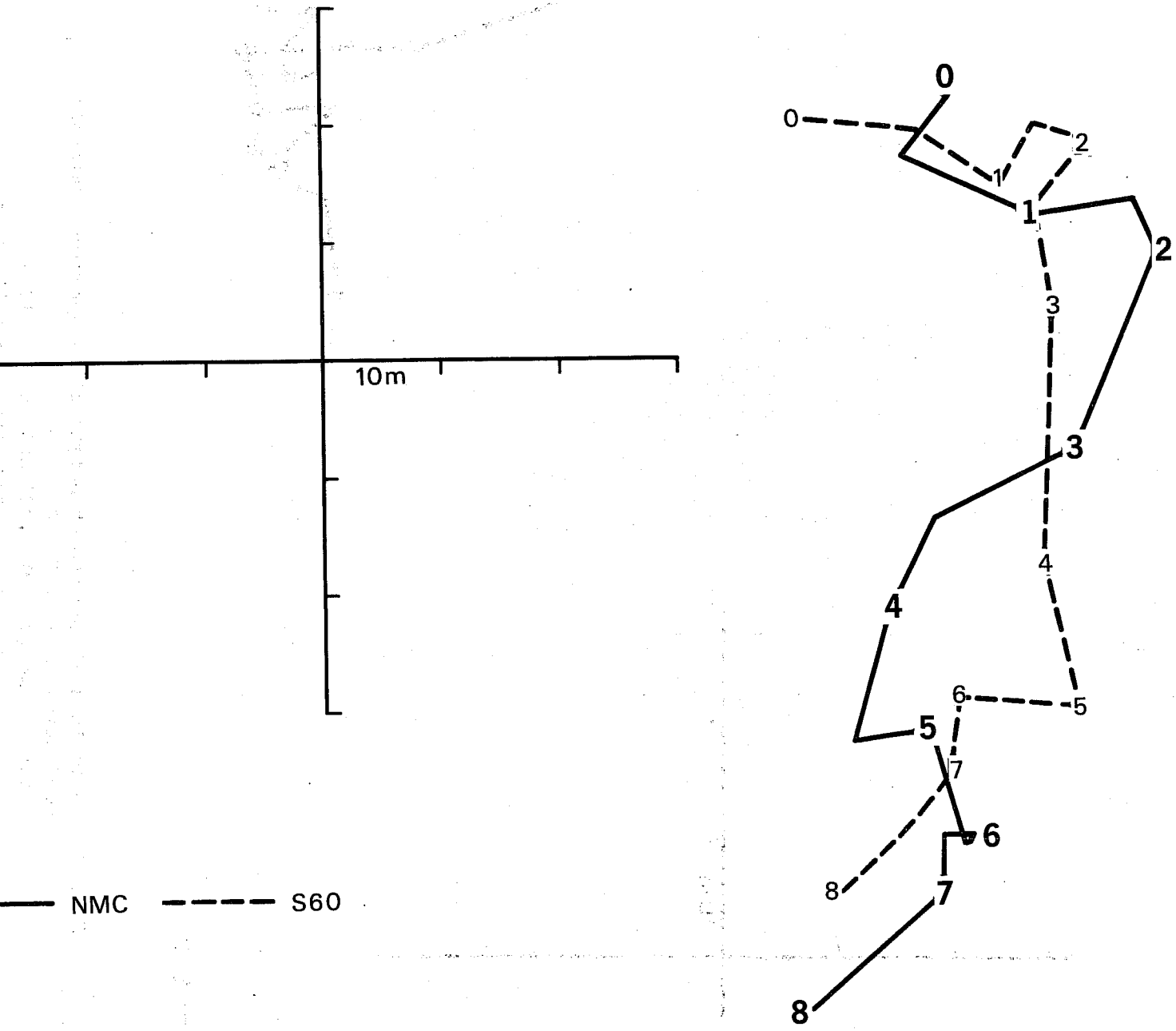

Fig. 22 Harmonic dial for 500 mb height field spherical harmonic coefficient M = 1, N = 5
Initial time (Day 0): 79011600, Unit : 10 M
Numbers are the time in days from the initial time

We have been trying to carry out these experiments in as stringent a manner as possible, but for some practical reason two slightly different data-sets have been used (see Table 2). It is not expected that this will have had an influence on the results and it will certainly not affect our conclusions. Two smaller errors in the programs were found after the experiments were finalised. The satellite temperatures obtained a smaller weight than they should have had (the thickness errors were assumed to be 3 times as large) and the humidity was slightly underestimated. Since these errors were made in all the experiments, they will not affect our comparisons, except for the experiments with and without satellite data. The major differences in that comparison are caused by the satellite winds.

In evaluating the different experiments we will concentrate on the way the particular blocking phenomenon is being predicted. We will also present some general statistics (RMS and correlation coefficient stratified in different wavenumber domains).

5.1 Resolution experiments

We will in this sub-section describe 6 different resolution experiments. One of the integrations is an N48 resolution grid point model, the other ones are spectral models with different resolutions, Fig. 23. Table 3 and Table 4 show the RMS and the anomaly correlation for every second day for the total field as well as for the long waves. It can be seen that the predictability is being reduced when the resolution is decreased but also that there is very little difference in the accuracy of the 3 models with the highest resolution. Another interesting observation is also the great similarity between the high resolution spectral integration and the grid point integration. This is illustrated in Table 5 which shows that the difference between N48 and T63 even after 4 days is not larger than the initial difference between the ECMWF and NMC analyses.

Notation of experiment	Model specification	DAY 2 Total	DAY 2 1-3	DAY 4 Total	DAY 4 1-3	DAY 6 Total	DAY 6 1-3	DAY 8 Total	DAY 8 1-3
R 47	Grid point N48-L15	53	33	75	50	105	50	100	67
S 60	Spectral P63/ 58/74-L15	53	33	83	50	111	58	100	67
T 46	Spectral T63-L15	53	33	78	50	111	56	100	68
T 45	Spectral T40-L15	53	33	78	50	111	56	114	67
T 14	Spectral T21-L15	64	42	97	67	111	61	117	78
T 17	Spectral T21-L5	78	44	119	78	139	94	164	111

Table 3

Table gives RMS-error for the total field (1000-200 mb and 20^{o}N-82.5^{o}N) for every 2nd day. **Unit m.**
The error is given for the total field and for the long-waves (wavenumber 1-3) separately. The climatological variance (norm) is 89 m for the long waves and 122 m for the total field. Verification has been carried out as NMC operational analyses . The initial "error" is 33 m for the total field and 22 m for the long waves.

Notation of experiment	Model specification	DAY 2 Total	DAY 2 1-3	DAY 4 Total	DAY 4 1-3	DAY 6 Total	DAY 6 1-3	DAY 8 Total	DAY 8 1-3
R47	Grid point N48-15	0.91	0.95	0.81	0.89	0.68	0.88	0.70	0.80
S60	Spectral P63/ 58/74-L15	0.93	0.95	0.75	0.88	0.65	0.86	0.69	0.84
T46	Spectral T63-L15	0.91	0.95	0.79	0.89	0.65	0.84	0.69	0.85
T45	Spectral T40-L15	0.91	0.95	0.78	0.89	0.60	0.83	0.53	0.75
T14	Spectral T21-L15	0.85	0.93	0.66	0.78	0.54	0.75	0.44	0.64
T17	Spectral T21-L 5	0.84	0.91	0.68	0.86	0.60	0.79	0.53	0.42

Table 4

The same as for Table 3 but for the correlation coefficient (anomaly correlation).

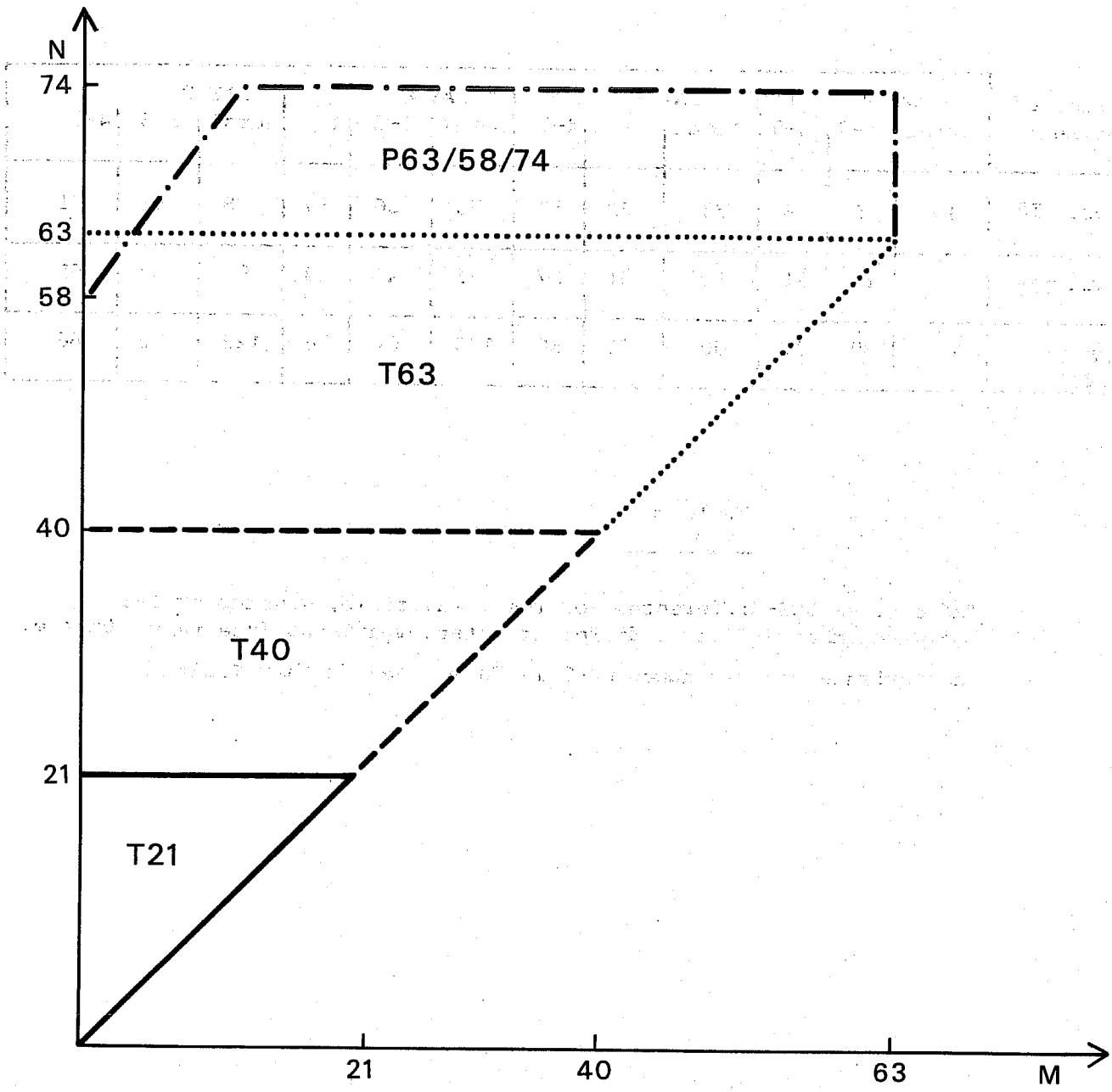

Fig. 23 5 different spectral resolutions. The size of the area is proportional to the number of degrees of freedom for each resolution.

Notation of experiment	DAY 2			DAY 4			DAY 6			DAY 8		
	Total	1-3	4-9	Total	1-3	4-9	Total	1-3	4-9	Total	1-3	4-9
N48 vs. T63	17	8	8	33	22	19	55	36	30	78	58	41
T63 vs. T40	19	11	11	50	31	27	81	47	48	97	60	55
P63/58/74 vs. T21	61	39	37	100	71	56	106	64	76	122	82	86

Table 5

Table gives RMS-differences for the total field, wavenumber 1-3 and wavenumber 4-9 for 3 different intercomparisons (see text). Unit m.

The variance for wavenumbers 4-9 is 70 m. See further Table 3.

Notation of experiment		DAY 0 observed			DAY 2			DAY 4			DAY 6			DAY 8		
		Total	1-3	4-9	Total	1-3	4-9	Total	1-3	4-9	Total	1-3	4-9	Total	1-3	4-9
	Observed NMC	278	85	56	258	65	45	267	59	53	254	56	52	250	48	43
R 47	Grid point N48-L15				242	60	40	246	61	37	242	45	47	242	43	40
S 60	Spectral P63/58/ 74-L15				246	60	43	246	59	43	233	50	39	216	39	33
T 46	Spectral T63-L15				242	60	43	242	55	44	225	45	37	213	36	30
T 45	Spectral T40-L15				233	57	39	233	55	38	213	37	33	217	32	28
T 14	Spectral T21-L15				229	58	37	229	53	38	196	32	35	200	28	39

Table 6

Table 6 gives the observed and predicted kinetic energy for every 2nd day for the total field and for the long waves (wavenumber 1-3) and medium waves (wavenumber 4-9) separately. The kinetic energy has been integrated from 1000 - 200 mb and from 20^{o}N - 82.5^{o}N. Units $10KjM^{-2}$.

Available Potential Energy

Notation of experiment	Observed NMC	DAY 0 observed			DAY 2			DAY 4			DAY 6			DAY 8		
		Total	1-3	4-9	Total	1-3	4-9	Total	1-3	4-9	Total	1-3	4-9	Total	1-3	4-9
		400	78	32	431	79	28	444	85	24	424	86	23	444	79	21
R 47	Grid point N48-L15				396	63	23	396	69	21	417	65	23	444	60	21
S 60	Spectral P63/58/ 74- L15				396	60	20	389	69	21	396	65	16	431	53	18
T 46	Spectral T63-L15				396	63	23	389	69	21	403	55	18	424	48	24
T 45	Spectral T40-L15				382	61	24	382	66	21	403	59	18	403	48	21
T 14	Spectral T21-L15				375	55	23	361	55	22	375	50	18	368	45	21

Table 7

Same as Table 6 but for available potential energy (integrated between 850 - 200 mb).

On the other hand the differences between the highest and the lowest spectral resolution grow fast, and from 2 days onward this difference is greater than the actual RMS-error for the high resolution integration. Consequently the high resolution integration stays closer to reality through the whole 8 day integration than the low resolution to the high resolution.

Table 6 and Table 7 show the variation of kinetic energy and available potential energy in time. All models underpredict the kinetic energy, the more the lower the resolution is although the error is rather small for the grid point model. The underprediction of kinetic energy can be seen for all wave components in particular for the long waves. The values in the Tables are spot values, and some small fluctuations affect the results.

The models also underestimate the available potential energy, in particular the available potential energy of the long waves. This underestimation becomes successively worse with reductions in the resolution.

The prediction of the blocking high shows likewise a successive deterioration as resolution is being reduced. However, the prediction of the blocking phenomenon is qualitatively correct for all of the models in the sense that we predict the initial easterly movement of the block followed by a re-establishment of the block 40 - 50^{o} upstream around day 4 and day 5. The 500 mb forecast for the T21-L15 model and the corresponding NMC verification are presented in Fig. 24. This figure also shows the trajectory for the blocking high.

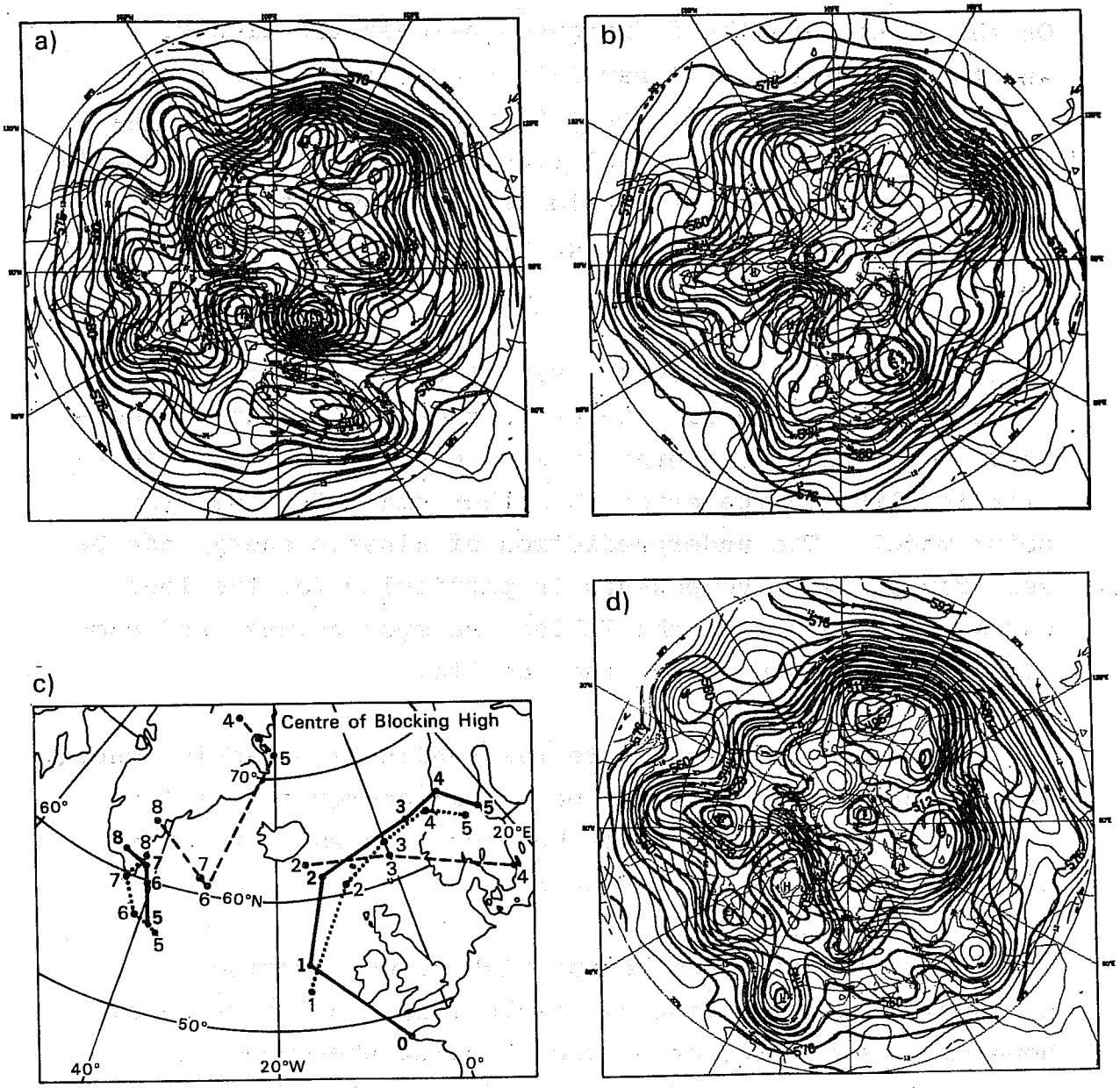

Fig. 24 Shows the 500 mb geopotential (full lines) and temperatures (thin (lines) for (a) 4 day forecast with T21-L15 (b) 8 day forecast (c) full lines observed trajectories for the blocking high day by day, dotted lines predicted by the high resolution spectral model, dashed lines predicted by the T21-L15 model day by day (d) observed 500 mb at 24/1 00Z.

5.2 Parameterisation experiment

The parameterisation experiment has been done by comparing 2 different parameterisation schemes. The parameterisation schemes are given in Table 8. The first of the schemes, EC(a), uses a parameterisation developed for climate simulations and is in essence equivalent to the scheme given by Manabe et al (1974). This scheme uses climatologically given clouds and uses drag coefficients independent of stability and friction height. The second scheme, EC(b), is the one developed for the ECMWF operational model and described by Tiedtke et al (1979). Scheme EC(b) has been used for all the other experiments described in this study and it is also being used operationally at ECMWF. A more extensive comparison between these two schemes has been published by Hollingsworth et al (1979).

Table 9 summarises the result from the parameterisation experiment. It is found that the scheme EC(b) is superior in this case, while in the comparison by Hollingsworth et al (1979) only a very small improvement could be noticed. The error growth is much faster for EC(a) and in particular the long waves have a much faster error growth. Both the kinetic and available potential energy fall off faster with time for this parameterisation scheme, in particular the available potential energy. The most likely explanation for this is the use of a climatological distribution of clouds in EC(a) which in a case of blocking will have a more harmful effect because on this occasion we have a very large deviation from climatology.

The prediction of the blocking high is also less good, in particular towards the end of the 8-day period where the blocking cell is successively filled out. The model is slowly working towards the more probable climatological state. The 500 mb forecast for the T40-L15 with EC(a) is shown in Fig. 25, together with the corresponding NMC verification. This figure also shows the trajectories for the blocking high.

TABLE 8

Survey of the parameterization schemes

Process	EC(a)	EC(b)
Large-scale condensation	Condensation, if relative humidity exceeds 80%	Condensation, if relative humidity exceeds $U=0.8+0.2e^{-7.0(1-\sigma)}$ Evaporation of rain
Convection		
Dry convection	Dry convective adjustment	Mixing by vertical diffusion of sensible heat, moisture and momentum
Moist convection	Moist adiabatic adjustment	Deep convection by Kuo convection scheme
Turbulent motion		
Horizontal diffusion	Non-linear, fourth order in space	Non-linear, fourth order in space
Vertical surface fluxes	$F_X \sim C_d(V_n)(X_h - X_s)$ C_d = const.	$F_X \sim C_d(V_h)(X_h - X_s)$ $C_d = C_d(R_i, \frac{h}{z_o})$ (R_i = Richardson number)
Vertical fluxes above surface layer	Vertical diffusion assuming K=K(z) with K=0 for z > 2500 m	Vertical diffusion assuming $K=K(R_i, \ell)$ and $\ell=\ell(z)$
Radiation	Absorber: Zonal means of H_2O, CO_2, O_3, clouds (specified at 3 levels)	Feedback between moisture (clouds) and radiation.
Surface values		
T_s Ocean	Prescribed	As in EC(a)
T_s Land	Diagnosed (energy balance equation)	Predicted
Soil moisture	Predicted	As in EC(a)
Snow	Predicted	As in EC(a)

	DAY 2		DAY 4		DAY 6		DAY 8	
	Total	1-3	Total	1-3	Total	1-3	Total	1-3
RMS	62	38	88	59	121	83	128	93
corr. coeff.	0.89	0.94	0.71	0.81	0.46	0.62	0.37	0.50
kinet. energy	240	56	228	44	208	35	212	32
available pot.energy	360	51	347	52	353	52	353	40

T 40 - L 15 parameterization EC(a)

	DAY 2		DAY 4		DAY 6		DAY 8	
	Total	1-3	Total	1-3	Total	1-3	Total	1-3
RMS	53	33	78	50	111	56	114	67
corr. coeff.	0.91	0.95	0.78	0.89	0.60	0.83	0.53	0.75
kinet. energy	233	57	233	55	213	37	217	32
available pot.energy	382	61	382	66	403	59	403	48

T40 - L15 parameterization EC(b)

Table 9

Model Specification : RMS(m) correlation coefficient for the total field (1000 - 200 mb and 20^{o}N - 82.5^{o}N) for every 2nd day.

The error is given for the total field and for the long waves (wavenumber 1-3) separately.

The table also gives the corresponding values for predicted kinetic energy and available potential energy.

The same units as in Tables 6 and 7.

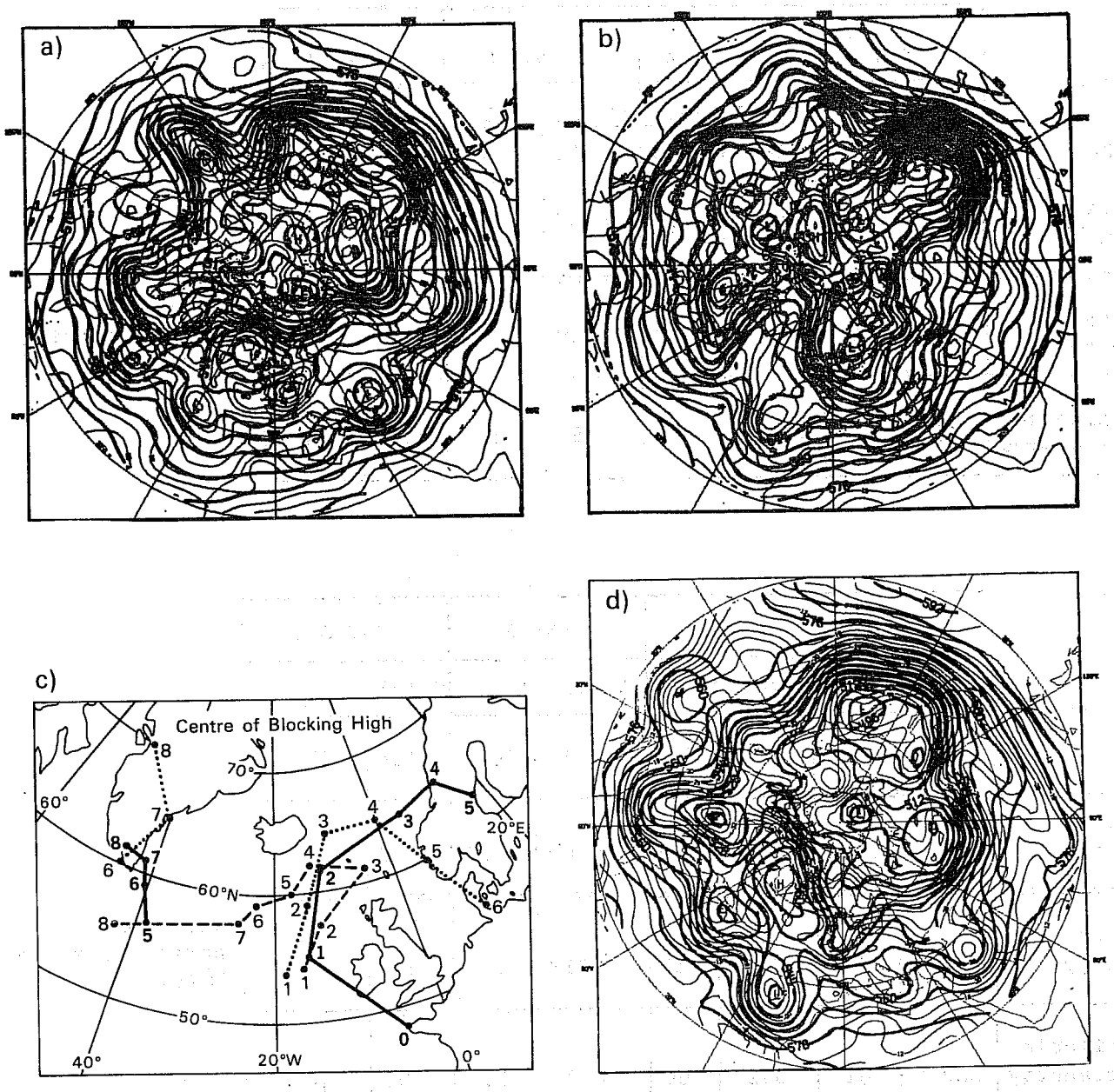

Fig. 25 Shows the 500 mb geopotential (full lines) and temperatures (thin lines) for (a) 4 day forecast with EC(a) (b) 8 day forecast with EC(a) (c) full lines observed trajectory for the blocking high day by day, dotted lines predicted by EC(b), dashed lines predicted by EC(a) (d) observed 500 mb at 24/1 00Z.

5.3 The effect of an equatorial boundary

The effects of an equatorial wall have been investigated by Miyakoda (1973) and Baumhefner (1972). Arpe et al (1977) have also carried out a study where the analysis at the southern hemisphere was replaced by climatology. These studies show that there is an observable effect after 3 - 4 days which grows fast to a substantial value beyond 7 - 8 days. The effect of the equatorial wall or of the lack of data at the southern hemisphere spreads in a very complicated way and after 7 - 8 days the largest errors are found in areas where the meteorological activity is most intense. Even if the previous forecasts differed substantially after 7 - 8 days, their errors compared to reality were about the same.

In this particular case we have the unique possibility to study the effect of a meteorological situation where we have found a very high predictability. In this situation, since we are using FGGE level III-b data, we have also substantially better data at the southern hemisphere.

Recently Somerville (1979) found that a boundary at the equator reduces the predictability of the long waves. The long waves are likely to be affected first because of their dimensions and their high group velocities. It is also likely that the effect will vary from case to case due to the flow configuration at the boundary. For this particular case the effect was considerable and as can be seen from Table 10 the long waves were influenced noticeably already after 2 days. The effect on the block Fig. 26 is relatively small, although the behaviour at the end of the prediction differs considerably.

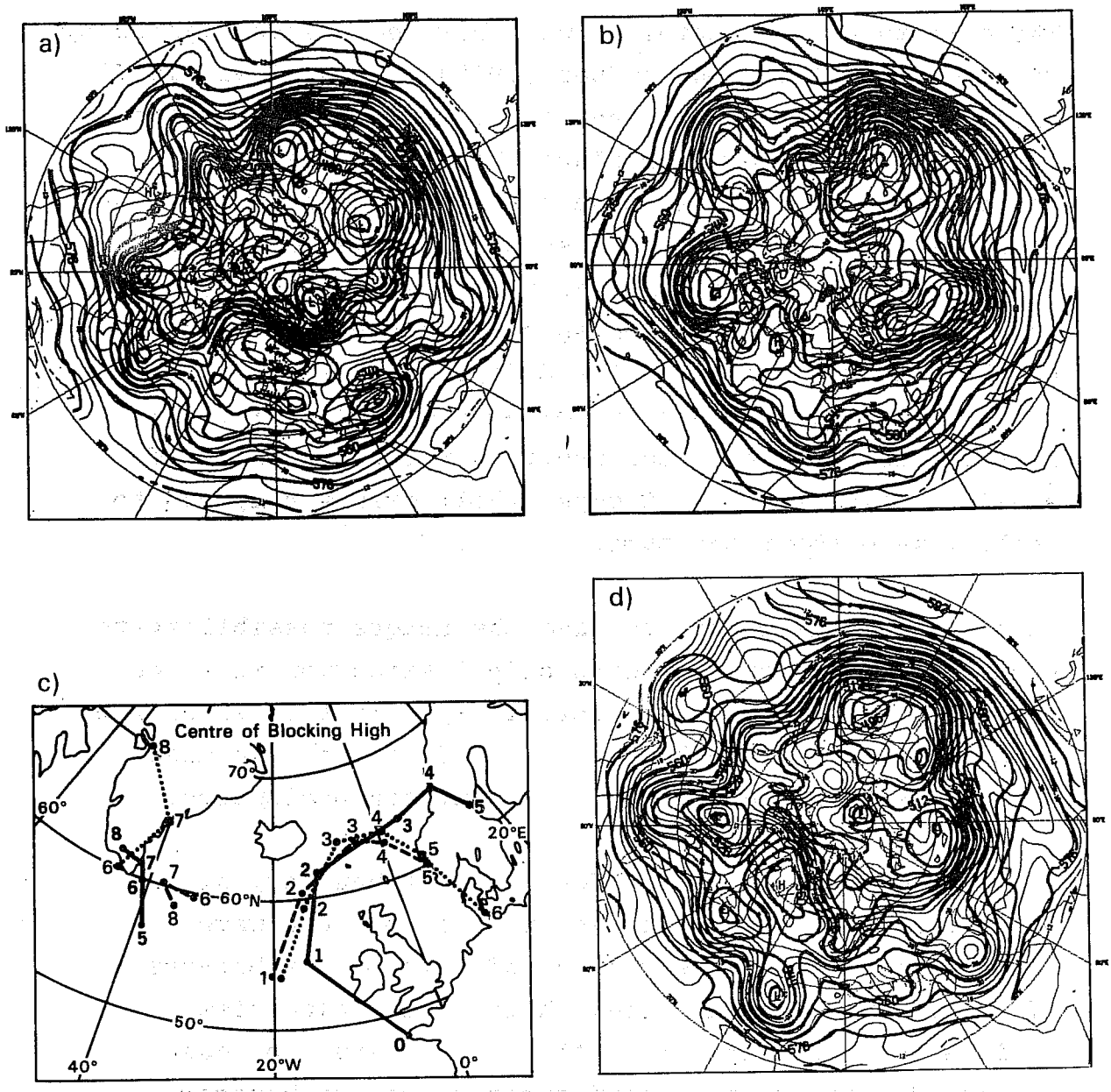

Fig. 26 Shows the 500 mb geopotential (full lines) and temperatures (thin lines) for (a) 4 day forecast with hemispheric model, (b) 8 day forecast with hemispheric model (c) full lines observed trajectories for the blocking high day by day, dotted lines predicted by the global model, dashed lines predicted by the hemispheric model (d) observed 500 mb at 24/1 00Z.

Notation of experiment	Model Specification	DAY 2 Total	DAY 2 1-3	Day 4 Total	Day 4 1-3	DAY 6 Total	DAY 6 1-3	DAY 8 Total	DAY 8 1-3
T 45	T40-L15 global	53 0.91	33 0.95	78 0.78	50 0.89	111 0.60	56 0.83	114 0.53	67 0.75
T 15	T40-L15 N.H.	61 0.89	44 0.91	94 0.71	67 0.78	114 0.53	69 0.70	117 0.53	78 0.65

Table 10

RMS and correlation coefficient for the total field (1000 - 200 mb and 20°N - 82.5°N) for every 2nd day. The error is given for the total field and for the long waves (wavenumber 1-3) separately. Results are given for a global integration (top) and a northern hemispheric integration (bottom)

Model Specification	DAY 2 Total	DAY 2 1-3	DAY 4 Total	DAY 4 1-3	DAY 6 Total	DAY 6 1-3	DAY 8 Total	DAY 8 1-3
N 48 - L 15 S A T	53 0.91	33 0.95	75 0.81	50 0.89	105 0.68	50 0.88	100 0.70	67 0.80
N 48 - L 15 NOSAT	59 0.89	36 0.94	89 0.74	64 0.83	116 0.60	64 0.78	117 0.58	74 0.71

Table 11

RMS-error and correlation coefficient

For further explanation see Table 3

5.4 The effect of initial data

An alternative data set was obtained from a parallel data assimilation experiment which also started from 13/11/1979 00Z and from climatology. From this assimilation sequence all satellite temperatures as well as satellite winds were eliminated. This case has been studied elsewhere, Bengtsson (1979) and we will here only summarise the result in Table 11 and Fig. 27. Due to the fact that a too high error was assigned to the satellite temperatures (4 - 6^{o}) this impact study essentially measures the impact of satellite winds.

6. EXPERIMENTS WITH QUASI-GEOSTROPHIC MODELS

It may be of some interest to carry out some experiments with a few other and much simpler models to see their prediction performance on a case like this. Fig. 28 summarises the 4-day prediction with a barotropic model (with and without a free upper surface) as well as prediction by a quasi-geostrophic model. The quasi-geostrophic prediction in the operational forecast by the Swedish Meteorological and Hydrological Institute's 6-layer model is based on operationally received data. For a model description see Moen (1975). The horizontal resolution for the barotropic models was 381 km and for the quasi-geostrophic model 300 km at 60 ^{o}N respectively.

The 500 mb geopotential is given for day 4 together with the trajectories for the blocking high, Fig. 28. It is not very likely that the differences in data would be significant during the first 4 days while the differences between these forecasts and the reference integrations in Section 4 are due to model differences.

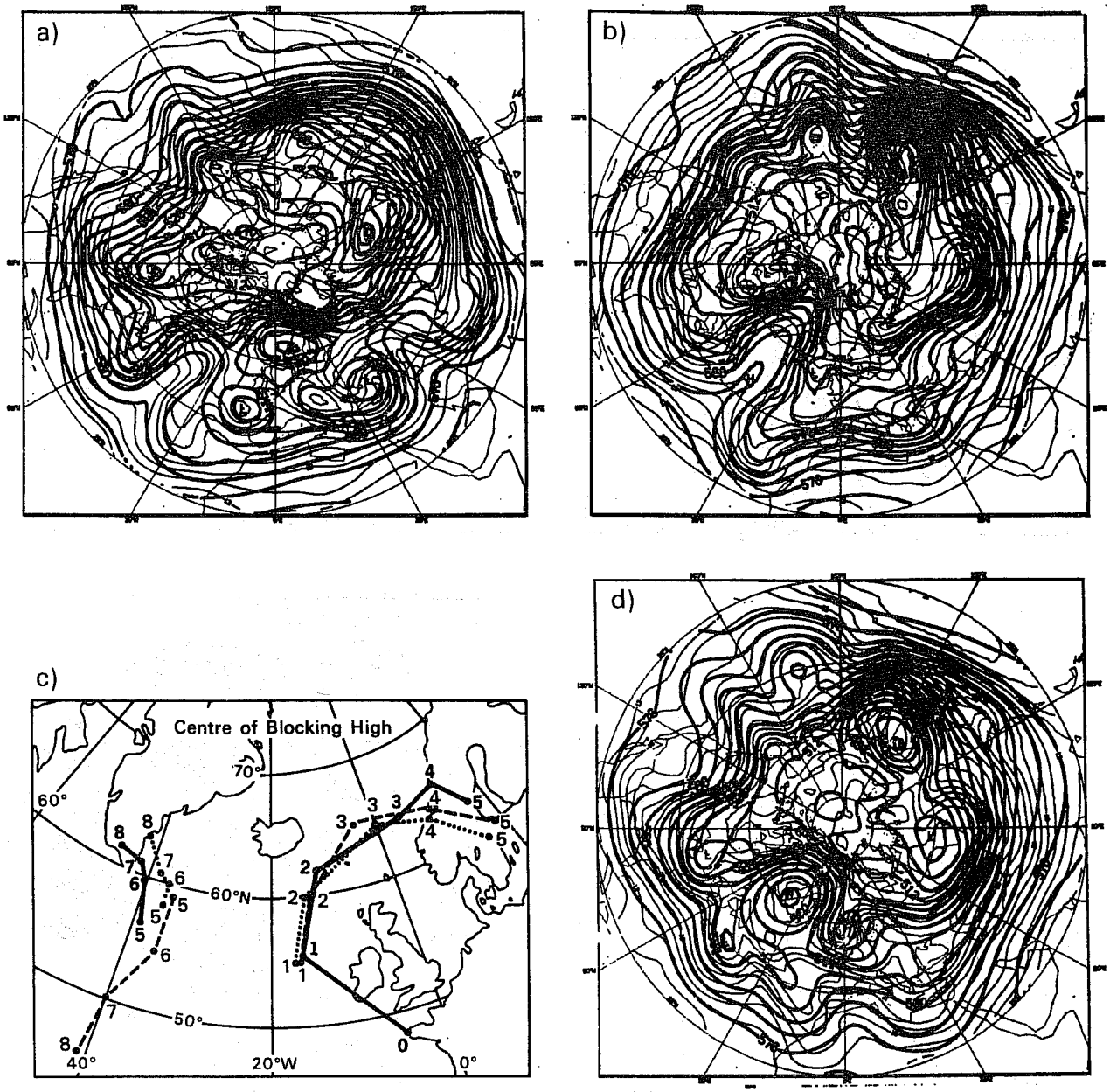

Fig. 27 Shows the 500 mb geopotential (full lines) and temperatures (thin lines) for (a) 4 day forecast with the NOSAT model (b) 8 day forecast with the NOSAT model (c) full lines observed trajectories for the blocking high day by day, dotted lines predicted by the SAT-model, dashed lines predicted by the NOSAT model (d) 8 day forecast with SAT-model.

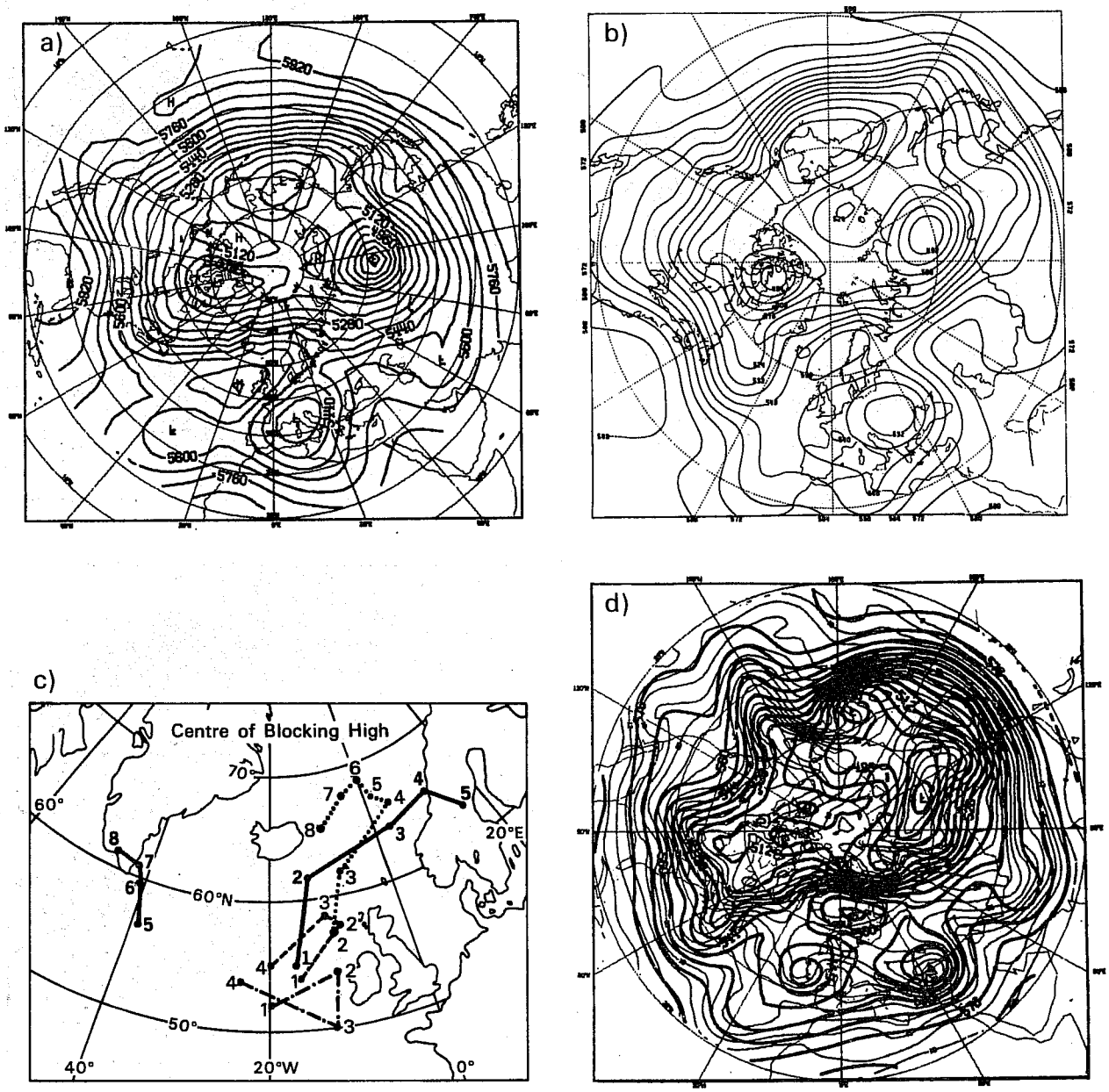

Fig. 28 Shows the 500 mb geopotential for (a) 4 day forecast with the barotrophic model (with an upper free surface) (b) 4 day forecast with the Swedish Meteorological and Hydrological Institute's 6 layer quasi-geostrophic model (c) full lines observed trajectories for the blocking high day by day, dotted lines predicted by the baroclinic quasi-geostrophic model, dashed lines predicted by the barotropic model with a free surface, dash-dotted lines predicted by the baroclinic model with a fix surface (d) 4 day forecast with high resolution grid point model. For verification see 3b

Nobody would dispute that progress has been made in NWP since the first numerical forecasts were made with the barotropic model some 30 years ago. In spite of the fact that quasi-geostrophic models can still be quite good for short range forecasts the efforts and work which has gone into the design of high resolution primitive models have certainly been worth the effort.

7. CONCLUSION

It is difficult for many reasons to draw firm conclusions for a study which is as limited as this one. However, the result of the study is positive in the sense that efforts in improving both the data, parameterisation and numerical resolution, all have a positive impact on the predictability. There is no hesitation either by inspecting results by simpler models that all efforts which have gone into improving numerical weather prediction through the years have been worthwhile. As far as the prediction of blocking is concerned, the following remarks can be made:

(i) We can have a cautious optimism about the predictability of significant large scale weather episodes such as blocking on a time-scale of 10 days.

(ii) It seems clear, although even very simple systems can produce flow patterns which remind about blocking that we need a high resolution model with realistic parameterisation in order to obtain useful predictability of blocking on a timescale more than 5 days.

(iii) The results from the resolution experiment suggest that the action of non-Newtonian forces, e.g. the interaction between travelling small scale eddies and the quasi-stationary systems are essential and a Newtonian approach to blocking can possibly only give a very crude picture about the real phenomenon.

(iv) There is no necessary increase in the long waves during blocking, in fact in this particular case the amplitudes of the ultra long waves were reduced by as much as 40% during the build up of the blocking pattern.

Acknowledgement

The author wishes to acknowledge assistance given by staff members of the Research Department of ECMWF to carry out the experiments presented in this article. He wishes specifically to thank M. Jarraud and U. Cubasch for carrying out all the spectral integrations.

The Swedish Meteorological and Hydrological Institute has provided results from their operational model and the author is grateful for this contribution.

References

Arpe, K., et al., 1977 :
The effect of replacing southern hemispheric analyses by climatology on medium range weather forecasts. European Centre for Medium Range Weather Forecasts, Internal Report No. 2, 40 p. Available from ECMWF.

Baumhefner, D.P., 1972:
Further experimentation with an imposed southern boundary for large-scale numerical weather prediction. J.Atm.Sci. 29, 768-772.

Bengtsson, L., 1978:
Growth rate and vertical propagation of the initial error. Tellus 23, 323-334.

Bengtsson, L., 1979:
Problems of using satellite information in numerical weather prediction.
Use of Data from Meteorological Satellites. Technical Conference Lannion, France, 17-21 September 1979. European Space Agency 14 p.

Burridge, D.M., and Haseler, J., 1977:
A model for medium range weather forecasting. European Centre for Medium Range Weather Forecasts, Technical Report No. 4- 45 p. Available from ECMWF.

Charney, J. et al., 1966:
The feasibility of global observations and analysis experiments. Bull. Amer. Met. Soc., 47, No. 3, 200-220.

Charney, J., and DeVore, J. 1979:
Multiple flow equilibria in the atmosphere and blocking. J. Atmos. Sci., 36, 1205 - 1216.

Druyan, L.M. et al., 1975:
Extended-range forecasts with the GISS model of the global atmosphere. Mon. Wea. Rev. 103, 779-795.

Döös, B.R., 1970:
Numerical experimentation related to GARP. GARP Publication Series No. 6, 68 p.

Hollingsworth A., et al., 1979:
Comparison of medium range forecasts made with two parameterisation schemes. European Centre for Medium Range Weather Forecasts, Technical Report No. 13, 214 p. Available from ECMWF.

Lambert, S.J., and Merilees, P.E. 1978: A study of planetary wave errors in spectral numerical weather prediction model. Atmosphere-Ocean 16, 197-211.

Lorenz, E.N. 1968:
On the range of atmospheric predictability. Proc. First Statistical Meteorological Conference. Amer. Met. Soc., 11-19.

Lorenz, E.N., 1969a:
Three approaches to atmospheric predictability. Bull. Amer. Met. Soc., Vol. 50, No.5, 345-349.

Lorenz, E.N. 1969b:
The predictability of a flow which possesses many scales of motion. Tellus, Vol. 21, No. 3, 289-307.

Lorenc, A., et al., 1977:
The ECMWF analysis and data assimilation scheme. Analysis of mass and wind fields. European Centre for Medium Range Weather Forecasts, Technical Report No. 6, 46 p. Available from ECMWF.

Miyakoda, K., and Umscheid, L., 1973:
Effects of an equatorial wall of an atmospheric model. Mon. Wea. Rev. 101, 603-616.

Miyakoda, K. et al., 1972:
Cumulative results for extended forecast experiments. I. Model performance for Winter Cases. Mon. Wea. Rev.,50, Rev. 100, 836-855.

Moen, L. 1975:
A multi-level quasi-geostrophic model for short range weather predictions. SMHI Rapporter Meteorologi och Klimatologi Nr. RMK (1975) 33 p. Available from the Swedish Meteorological and Hydrological Institute.

Rex, D.F., 1950a:
Blocking action in the middle troposphere and its effect upon regional climate. I. An aerological study of blocking action. Tellus, 2, 196-211.

Rex, D.F., 1950b:
II. The climatology of blocking action. Tellus, 2, 275-301.

Robinson, G.D., 1967:
Some current projects for global meteorological observation and experiment. Quart. J. Roy. Met. Soc., Vol.93, No. 398, pp. 409-418.

Smagorinsky, J., 1969:
Problems and promises of deterministic extended range forecasting. Bull. Amer. Met. Soc., Vol. 50, No. 5, 286-312.

Somerville, R., 1979: Predictability and prediction of ultra-long planetary waves. Fourth Conference on Numerical Weather Prediction, Silver Spring, Maryland, U.S.A., October 29-November 1, 1979. 4 p.

Temperton, C., and Williamson, D., 1979:
Normal mode initialisation for a multi-level grid point model. European Centre for Medium Range Weather Forecasts, Technical Report No.11, 91 p. Available from ECMWF.

Tiedtke, M., et al., 1979:
ECMWF Model - Parameterisation of sub-grid scale processes. European Centre for Medium Range Weather Forecasts, Technical Report No. 10, 46 p. Available from ECMWF.

Thompson, P.D., 1961:
Numerical Weather Analyses and Prediction. New York, Macmillan.